# Transition Edge Sensors with Sub-eV Resolution And Cryogenic Targets (TESSERACT) FRANCE

Julien Billard[1], Jules Gascon[1], Stefanos Marnieros[2], and Silvia Scorza[3]

[1]Univ Lyon, Université Lyon 1, CNRS-IN2P3, IP2I-Lyon, F-69622 Villeurbanne, France
[2]Université Paris-Saclay, CNRS-IN2P3, IJCLab, 91405 Orsay, France
[3]Univ. Grenoble Alpes, CNRS, Grenoble INP, LPSC-IN2P3, 38000 Grenoble, France

October 2, 2023

## Contents

# 1 Searching for Light Dark Matter with TESSERACT

## 1.1 Scientific Motivations

Elucidating the identity of dark matter (DM) is one of the most compelling problems of high energy physics. For decades, theoretical and experimental probes have been focused on the weak scale in the search for answers to nature's deepest mysteries, including the identity of DM. This is understandable: in addition to connecting the DM problem to the question of the natural mass scale for the Higgs boson, the DM relic abundance falls out naturally from the freeze-out paradigm. However, a lack of evidence for a thermally produced GeV-to-TeV mass-scale Weakly Interacting Massive Particles (WIMP) in direct detection experiments and at the Large Hadron Collider (see, e.g., Refs. [1], [2], [3], [4], [5], [6], [7]) has motivated a theoretical effort to develop new DM theories that are consistent with current experimental and observational bounds. Some general properties of DM particle candidates can be established already from observational evidence and numerical simulations alone. The DM particle is favoured to be *cold*, non-baryonic, should also be either absolutely stable (or extremely long lived) with only weak interactions[1] with itself or any other particles from the Standard Model. Also, the DM particle mass range can span nearly 50 orders of magnitude, from values as tiny as $10^{-21}$ eV (fuzzy DM) for bosons with de Broglie wavelength of the order of typical sizes of dwarf galaxies [8] up to the (reduced) Planck scale $\overline{M}_P \simeq 2 \times 10^{18}$ GeV (above which it is difficult to consider DM particles as elementary). This is as much as we can be fairly confident about the general properties of DM which, however, is only a first step towards identifying its real nature, since they can be easily satisfied by a wide range of specific particle candidates, or in fact classes of candidates. In particular, compelling models of new physics, including those of the dark sector, may naturally have mass below the weak scale. These paradigms of hidden sector DM include Hidden Valleys [9] with composite DM (whether dark mesons [10], atomic DM [11], or glueballs [12]), Asymmetric DM [13], supersymmetric hidden sector DM [14, 15, 16, 17], strongly interacting massive particles [18], and self-interacting DM [19, 20, 21]. Hidden sector theories have also given rise to new approaches to deep questions, such as models for baryogenesis [22, 23, 24] and "neutral naturalness" [25] solutions to the hierarchy problem.

## 1.2 TESSERACT at the Underground Modane Laboratory

The future TESSERACT (Transition Edge Sensors with Sub-eV Resolution And Cryogenic Targets) experiment aims at detecting light dark matter, from the proton mass down to a fraction of an electronvolt, via its interaction with ultra-sensitive new-generation cryogenic detectors. TESSERACT aims to be a ground-breaking experiment, representing a significant paradigm shift in relation to the current state of the art by considerably extending its light dark matter search mass range as illustrated in Fig. 1. Indeed, it aims to probe DM over 12 orders of magnitude in mass, using 1) **sub-eV energy thresholds** kinematically allowing to explore DM particle masses down to the (sub-)eV-scale, 2) **multi-target detectors**: $Al_2O_3$, $SiO_2$ GaAs, LHe, Ge and Si, to probe both nuclear (NRDM) and electronic (ERDM) recoil dark matter interactions, and 3) a **technology enabling DM interactions to be identified from** those arising from the **radioactive and instrumental backgrounds**. The combination of these last three technological features is what makes TESSERACT unique with respect to the competing experiments, *e.g.* DAMIC [27] and CRESST [28], also searching for light dark matter

[1] here weak may stand for the familiar weak force, or instead some other (sub)weak force defined by some non-negligible coupling to the Standard Model (SM) particles.

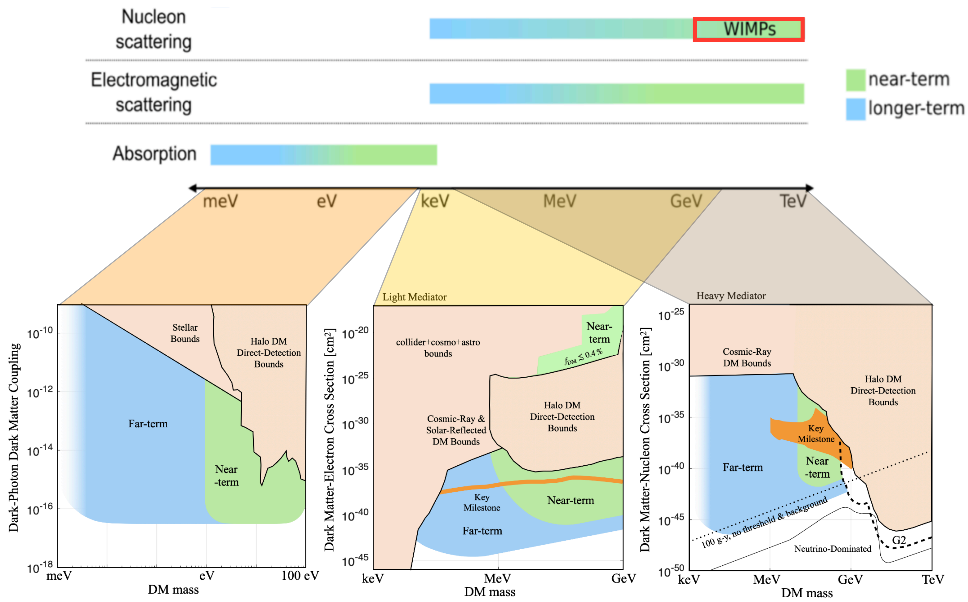


Figure 1: Illustration of the long and near term TESSERACT targeted search sensitivities probing light dark matter particles from the meV-scale up to the proton mass considering all types of DM interactions. Figure extracted and adapted from [26].

particles. As of today, the TESSERACT project is a US-only collaboration[2] funded through the Department of Energy (DOE) Dark Matter New Initiatives program since June 2020, which covers the transition from R&D to a project. Since early 2022, the French RICOCHET and EDELWEISS partners (the IN2P3 laboratories IP2I, LPSC and IJCLab) are discussing with the TESSERACT collaboration in order to 1) install a dedicated cryostat for TESSERACT at the underground Modane Laboratory (LSM), and 2) include the French semiconductor germanium bolometer technology to the initial TESSERACT science program including the SPICE (Sec. 2.3) and HeRALD (Sec. 2.4) detector technologies. TESSERACT is a single collaboration that will deliver the shielding, cryogenics, calibration tools, detectors, and project management necessary to achieve its scientific goals of leading the sub-GeV DM search over the next decade. The collaboration envisions to have two similar cryostats so as to allow for the operation of all three technologies, and allow some underground optimization of the detectors in one cryostat while still performing DM searches simultaneously in the second one.

The project planning phase aims to produce a fully defined experimental concept and project by the end of 2025 to lead the ultra-light DM search starting in 2026. The availability of a cryostat early in the first R&D phase is crucial, and for this the french collaborator propose to install and commission the TESSERACT Phase-1 cryostat at LSM. As more space at LSM becomes available in the coming future, the Phase-2 cryostat could be installed to ramp up the deployment of the different TESSERACTs technologies, building on the expertise and science results from the Phase-1 cryostat.

[2] **List of US institutes: Lawrence Berkeley National Laboratories, University California Berkeley, Argonne National Laboratory, Caltech, Texas A&M, Florida State University, UMass Amherst and University of Michigan State.**

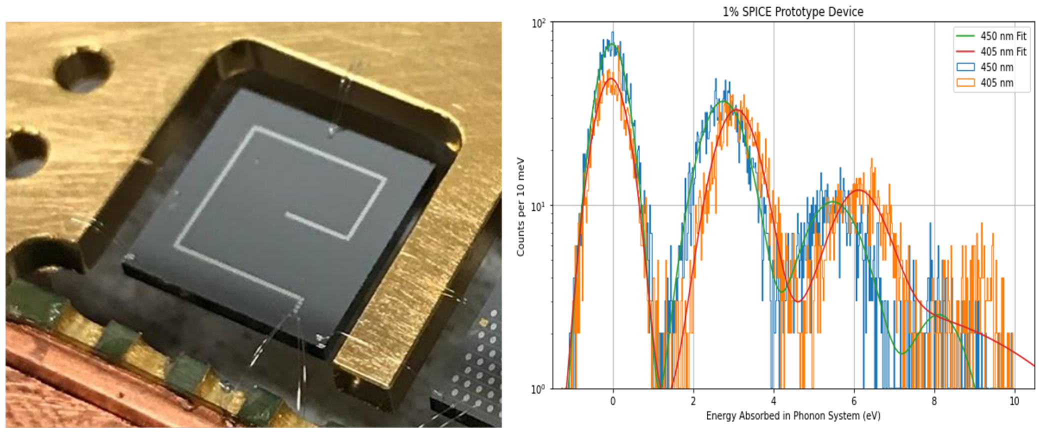


Figure 2: **Left:** Picture of a prototype 1 cm$^2\times$1 mm Si athermal phonon detector for TESSERACT. This prototype has a TES based athermal phonon sensor coverage of 1% and a critical temperature $T_C = 50$ mK. **Right:** Energy distributions obtained using the device shown in the left panel and optical photon calibrations with 405 and 450 nm wavelengths. Individual photon detection are clearly visible thanks to an unprecedented 273 meV phonon baseline energy resolution (RMS).

# 2 TESSERACT Detector Technologies

The detection of sub-eV energy depositions from nuclear recoils with $\leq 50$ MeV DM and electronic recoils for $\leq 1$ MeV DM with $\geq 100$ g.yr exposure combined with background rejection capabilities completely drives our experiment design. The proposed addition of the French semiconducting bolometer technology, based on the recent developments performed by the EDELWEISS and RICOCHET collaborations, will complement the initial SPICE (Sub-eV Polar Interactions Cryogenic Experiment) and HeRALD (Helium Roton Apparatus for Light Dark Matter) ones currently developed by the US collaborators. Indeed, all together, these detector technologies will be sensitive to both nuclear recoil interacting DM (NRDM) and electron recoil interacting DM (ERDM), with particle identification capabilities for background discrimination. The total mass for each target type will be between 10 g and 1 kg (depending on the target and R&D progress).

## 2.1 Athermal phonon Transition Edge Sensors

Athermal phonons produced directly via particle interaction, or indirectly via photon or $^4$He atom absorption, anharmonically decay to lower-frequency phonons in the bulk of the crystal. Since this decay rate scales with the phonon energy as $E^5$ [29], these bulk thermalization processes turn off around $\mathcal{O}(10\text{ K})$, and the low-energy phonons begin to free stream balistically. If the scattering surface is instrumented with superconducting phonon sensor arrays and a phonon has energy $\geq 4$ K, it can annihilate a Cooper pair within the superconducting Al collection fins, transferring on average about 50% of its energy into kinetic and potential energy of the resulting quasi-particles. These quasi-particles subsequently diffuse within the Al film until they encounter a trapping site in the Al and are lost, or they are transmitted into the small-volume TES attached to the edge of the fins, where they thermalize their remaining energy for measurement [30]. It has been shown that the baseline energy resolution, or equivalently the energy sensitivity, of the athermal phonon detector scales as

$$\sigma_E \propto V_{\rm det}^{1/2} T_c^3. \tag{1}$$

Equation 1 illuminates the design changes required to increase sensitivity; we must decrease the size of the detector to cm$^3$ scale from the 100 cm$^3$ traditionally used by SuperCDMS and EDELWEISS for higher mass DM. Additionally, we must lower $T_c$ from the 40-60mK range currently used in SuperCDMS to ideally 15-20 mK.

Figure 2 shows a recent TES based athermal phonon sensor detector prototype (left panel) together with its observed energy spectra following optical photon calibrations (right panel). The presented detector prototype is a 1 cm$^2$ $\times$ 1 mm Si crystal with 1% TES surface coverage and a $T_c$ of 50 mK. As one can see, first evidence for individual optical photon detection, with wavelengths of 405 and 450 nm, is clearly visible. Despite its 50 mK critical temperature, this prototype detector achieved an unprecedented baseline energy resolution of 273 meV (RMS) which could be further improved by about ten fold in lowering $T_c$ to the targeted 15-20 mK temperatures. Using Eq. 1, one can derive that a 1 cm$^3$ Ge (5.35 g) or Si (2.33 g) detector should achieve sub-eV energy thresholds using optimized TES based athermal phonon sensors as currently being developped by the TESSERACT collaboration.

## 2.2 Low-Energy Excess

In recent years, as cryogenic detector experiments successfully lowered their energy threshold below $\mathcal{O}(100)$ eV, a strong and yet-to-be-explained low-energy excess (LEE) background component has been observed [31]. Its level, observed in all low-threshold cryogenic experiments such as EDELWEISS [32, 33], CRESST [28], Ricochet [34], NuCLEUS [35], and SuperCDMS [36] is between $10^6$ and $10^8$ DRU at 100 eV recoil energy, hence several orders of magnitude larger than the expected radiogenic backgrounds. This low-energy excess represents a tremendous threat to many ongoing and upcoming low-threshold cryogenic DM experiments as it may very well overwhelm the putative targeted signals and dramatically limit their search sensitivities. Among some of the general properties of this excess (see [31] for a detailed review), the EDELWEISS/Ricochet collaborations have observed that these excess backgrounds do not ionize, hence their name "Heat-Only" (HO). As of today, the most likely hypothesis regarding this background origin is that it is either due to stress induced microfractures in the target crystal or at its interface with the phonon sensors. This suggests two important ways forward 1) find the origin of this background in order to suppress it, and 2) next generation of low-threshold cryogenic experiments must develop particle identification and/or active HO rejection techniques to achieve their expected DM sensitivities. **Both strategies are being investigated by the TESSERACT collaboration.**

Additionally, it is worth mentioning that superconducting quantum circuits (q-bits) see anomalously short decoherence times partially due to high density of quasiparticles (broken Cooper pairs due to energy depositions) that decrease as a function of time [37], in a similar fashion to the low-energy excess observed in all low-threshold cryogenic experiments [31]. There is therefore possibly a highly mutual benefit to solve this excess backgrounds at low energy for both light DM searches and quantum computer developments.

## 2.3 SPICE

**SPICE: $Al_2O_3$ and $SiO_2$ Detectors** – Since the vibrational energy scale in crystals is $\mathcal{O}(100)$ meV, for DM particle masses $m_{\rm DM} \leq \mathcal{O}$ (30 MeV), we can't use the simplifying approximation that the nucleus is free. Instead, we must think about the DM scattering coherently with the entire crystal producing a single phonon [38, 39, 40]. The kinematics of optical phonon production are favorable; due to their gapped nature, all of the kinetic energy of the DM can potentially be used for phonon creation. Additionally, since optical phonons modulate the electric dipole in polar crystals, they have strong couplings to infrared photons, and thus by extension, to all DM models that interact through a kinematically mixed dark photon.

To maximize sensitivity to these electromagnetically coupled DM models SPICE aims at developing an array of 1 cm$^3$ $Al_2O_3$ and $SiO_2$ detectors, instrumented on one face with athermal phonon sensors as presented in Sec. 2.1 with eV-scale energy thresholds and lower. The primary goal for these polar crystal detectors is to search for single optical phonons produced by electromagnetically interacting DM via scattering (3 keV $\leq m_{\mathrm{DM}} \leq$ 1 MeV) and via absorption (100 meV $\leq m_{\mathrm{DM}} \leq$ 1 eV). Backgrounds that directly interact with a TES/athermal phonon sensor, like stress-induced microfracture events within the athermal phonon sensor itself, are expected to be distinguishable in multiple ways. First, the athermal phonon collection time, $\tau_{\mathrm{collect}}$, is purposefully designed to be two times larger than $\tau_{\mathrm{sensor}}$. As such, events that deposit all of their energy within the TES can be distinguished from crystal interactions. Second, we can instrument each pixel with 2 separately read-out phonon sensor arrays; crystal events deposit energy nearly equally in the two arrays due to the low sensor coverage factor, while background events that interact with a single sensor would be trivially separable. Figure 3 (left panel) shows a picture of a first $\sim$ 10 g $Al_2O_3$ prototype detector currently being tested by the TESSERACT collaboration.

**SPICE: GaAs scintillation Detector** – Due to its small bandgap (1.52 eV), GaAs is ideally suited to search for inelastic ERs from electromagnetically coupled DM that is scattered ($m_{\mathrm{DM}} \geq$ 1 MeV) or absorbed ($m_{\mathrm{DM}} \geq$ 1.5 eV). In our detector concept, each 1 cm$^3$ GaAs detector is instrumented with athermal phonon sensors on its surface, and inside an optical cavity with a 1 cm$^2$ $\times$ 1 mm thick instrumented Ge crystal that serves as an infrared photon collector (see Fig. 2 - left panel). Due to its world-leading 60% quantum efficiency for a cryogenic scintillator [41], on average nearly 12% of the total ER energy ends up in photon energy, a large fraction of which will be absorbed and sensed by the photon sensor. Requiring a coincidence of signals to differentiate signal from backgrounds is standard practice for high-mass DM searches; in particular our setup certainly builds upon the design strategies of CRESST [42]. However, there are 2 significant differences. First, GaAs has a scintillation yield of about 125 ph/keV which is ten times larger than the one of $CaWO_4$ [41]. Secondly, GaAs has similar bandgaps as Ge and Si crystals and is therefore focused on finding an electronic recoil signal in the presence of lower yield backgrounds, including zero yield backgrounds (like micro-fractures) which is nowadays limiting CRESST performance. Considering the TES based athermal phonon sensor performance described in Sec.2.1 and the GaAs light yield, we expect to reject low-energy excess events down the eV-scale (single photon) recoil energy and extend ER/NR discrimination down to few tens of electronvolt hence allowing additional promising NRDM sensitivity that will be complementary with the semiconducting targets.

## 2.4 HERALD

While a strong motivation for a $^4$He target material is the low nuclear mass, superfluid $^4$He also has several material properties which aid in the readout of nuclear recoils. The first of these properties is the long lifetime and propagation distance of the phonon (and phonon-like 'roton') excitations. The second relevant material property is the low binding energy of $^4$He atoms at the liquid/vacuum interface. The atomic binding energy is so low (0.62 meV) that much of the phonon/roton population lies above this energy, such that a single signal phonon can individually eject a single $^4$He atom into the vacuum. This athermal 1-to-1 process is termed 'quantum

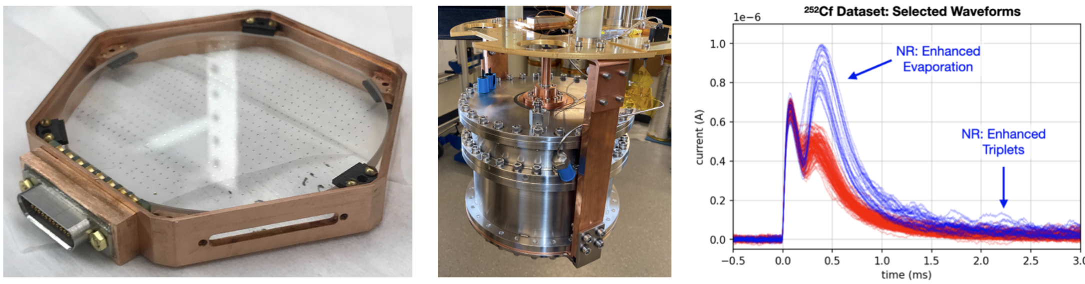


Figure 3: **Left:** Photo of a first $\sim$10 g $Al_2O_3$ prototype detector from the SPICE technology. **Middle:** Photo of the HERALD v0.1 detector mounted at the mixing chamber stage of a dilution cryostat at UMass Ahmerst. **Right:** Waveforms obtained with HERALD v0.1 from an $^{55}$Fe source (red) and a $^{252}$Cf neutron calibration (blue).

evaporation'. Several theoretical descriptions of this process have been given [43, 44, 45], and are in general qualitative agreement, predicting evaporation probabilities (per phonon incidence at the interface) of some 10s of percent. Experiments have shown broad consistency with theoretical prediction [46]. A sensor or sensor array in the vacuum region then receives a burst of ejected $^4$He atoms as the primary signal, and these atoms are sensed via their van der Waals binding energy to the sensor surface ($\sim$10 meV per adsorbed atom). The third relevant property is the helium superfluidity. As it is a liquid target, there should be no mechanical micro-fractures-like events within the helium itself contributing to "Heat-Only" (HO) backgrounds. Vibrational coupling is suppressed between the vessel walls and the superfluid helium, since objects move through pure superfluid helium without viscosity. Scattering events within the helium will produce rotons and phonons, yielding evaporated helium atoms to be detected on multiple athermal phonon pixels suspended above the liquid. Therefore, requiring coincidence between multiple pixels should drastically reduce HO backgrounds, even if individual pixels have HO events within them. Finally, superfluid helium is a very bright scintillator, with about 33% of ER energy going into prompt scintillation light. The NR light yield, while nonlinear with energy, is also very high: at energies measured so far we find a Lindhard quenching factor of 40%, corresponding to 13% of NR energy going into prompt scintillation. The scintillation signal will be another handle on discriminating ER events, NR events, and instrumental backgrounds for higher DM masses.

Early 2023, the HeRALD team successfully built and tested their first detector prototype [47]. Figure 3 middle shows a picture of the HERALD v0.1 prototype detector equipped with a Cs-based superfluid He film stopper and a photon/$^4$He detector, instrumented with athermal phonon TES, facing a 2.75 cm high and 6 cm diameter liquid $^4$He cell corresponding to about a total He target mass of 10 g. Right panel of Fig. 3 shows some first data from the HERALD v0.1 detector prototype exposed to a $^{252}$Cf neutron calibration source (blue waveforms) and to a $^{55}$Fe source emitting 5.9 keV X-rays (red waveforms). From these first data set, one can clearly appreciate the detection of the prompt scintillation signal followed by the one from the $^4$He quantum evaporation. Also, the comparison between the blue and red waveforms suggests that there is indeed an enhancement of the phonon/roton yield for nuclear recoils hence leading to a significant pulse shape discrimination between keV-scale ER and NR. For this present data, the detection threshold for energy in the $^4$He quasiparticle system is approximately 145 eV, which already corresponds to a very promising light dark matter mass sensitivity $m_{\rm DM} \geq 220$ MeV/c$^2$ [47].

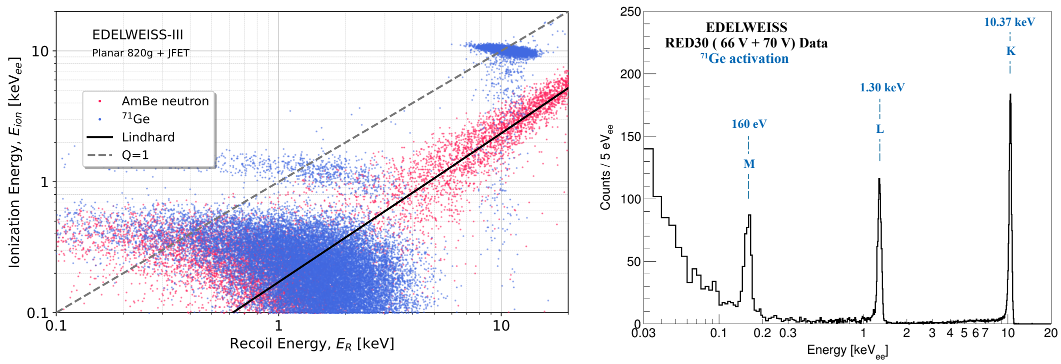


Figure 4: **Left:** Event distribution in the ionization versus recoil energy plane obtained with FID803 from the EDELWEISS-III collaboration operated at LSM. Black dots correspond to "low background" data with the K- and L-shell X-ray lines clearly visible, and the red dots correspond to neutron calibration data. Note that the large population of events below $E_{\rm ion} = 600$ eV$_{ee}$ and $E_R = 4$ keV corresponds to the so-called "noise-blob". **Right:** Energy spectrum recorded with a voltage bias of 66 V and 70 V following the $^{71}$Ge activation of the RED30 detector prototype at LSM. Figure taken from [33]

## 2.5 Cryogenic semiconducting bolometers

The EDELWEISS and SuperCDMS experiments have pioneered the use of cryogenic semiconductor crystals (Ge and Si) to search for DM particles. Following a particle's interaction in the detector medium, the induced recoil will release its energy by creating both phonons (heat) and charge carriers (ionization). To first order[3], the different measurable energy quantities are intertwined as follows:

$$E_{\rm ion} = Q(E_R)E_R \ , \quad E_{\rm NTL} = E_{\rm ion}\frac{V}{\epsilon} \ , \quad \text{and} \ \ E_{\rm heat} = E_R + E_{\rm NTL} = E_R\left[1 + Q(E_R)\frac{V}{\epsilon}\right] \quad (2)$$

where $V$ is the voltage bias and $\epsilon$ is the average energy required for an electron recoil to produce an electron-hole pair. $E_{\rm heat}$ and $E_{\rm ion}$ stand for the heat and ionisation energies, respectively. $E_{\rm NTL}$ is the additional Neganov-Trofimov-Luke heat energy produced by drifting the charge carriers across the crystal [48, 49]. The quenching factor $Q(E_R)$ is by definition equal to 1 for ER, between 0 and 0.3 for NR below 20 keV [50], and equal to 0 for "Heat-Only" backgrounds. It is worth highlighting that, in addition to the event-by-event discrimination, the simultaneous heat and ionisation energy measurements at V $\neq$ 0 also provides a direct measurement of the true nuclear recoil energy, hence avoiding any assumptions on the ionisation yield. Following Eq. (2), two operating modes can be considered.

**Low-voltage mode:** By operating the detector at low enough bias voltages ($\leq$4 V), such that $E_{\rm NTL} < E_R$ for nuclear recoils, the simultaneous measurement of heat and ionisation provides an event-by-event identification of the recoil type, hence allowing a highly efficient rejection of the dominant low-energy excess and gamma backgrounds. Residual gamma- and surface beta-backgrounds are further removed using active surface rejection, based on either veto electrodes or charge asymmetry, of the FID (Fully Interdigitised Design) from the EDELWEISS [51] experiments.

[3] We neglect here the phonon energy loss due to Frenkel defects and to charge trapping.

The EDELWEISS collaboration successfully achieved an average baseline energy resolution (RMS) of 400 eV and 220 eV$_{ee}$ for the heat and ionization channels, respectively, leading to the most efficient ER/NR discrimination at the time – see Fig. 4 (left panel). Thanks to this dual measurement, EDELWEISS has demonstrated a gamma and surface-beta rejection factors better than $< 2.5 \times 10^{-6}$ and $< 4 \times 10^{-5}$ at 90% C.L. respectively, while keeping a nuclear recoil acceptance of about 75% down to a nuclear recoil energy of 15 keV [51]. In 2016, thanks to these detector performance, though considerably limited by the "Heat-Only" (HO) excess background, the collaboration achieved leading exclusion limits on SI interactions for WIMP masses from 5 to 30 GeV/c$^2$ [52], and provided the first measurement of the cosmogenic activation rate of tritium in Ge above-ground [53]. The Ricochet CENNS experiment has considerably improved upon the previous EDELWEISS detector performance, now achieving heat and ionization energy resolution (RMS) of 20-to-50 eV and 30-to-40 eV$_{ee}$, respectively, thanks to its newly developed CryoCube detector technology (see Sec. 5.1). Such performance will allow in turn to achieve ER/NR rejection down to 100 eV and a $10^5$ HO background rejection down to about 250 eVnr [34]. The French TESSERACT partners will pursue this "low-voltage" approach in order to push for heat and ionization resolutions at the eV-scale in order to allow for highly sensitive NRDM sub-GeV DM searches, see Sec. 5.1.

**High-voltage mode:** By operating the detector at high voltage biases ($\geq$100 V), the cryogenic calorimeter is effectively turned into a charge amplifier of mean gain $(1 + Q(E_R)\frac{V}{\epsilon})$. As $E_{\text{heat}} \simeq E_{\text{ion}}$, event-by-event discrimination is no longer possible and an ionization yield model has to be assumed to convert the total heat energy into a nuclear recoil energy equivalent. This operation mode is highly beneficial to any DM searches looking for interactions with electrons instead of nuclei. First, the total phonon signal is amplified by a factor $(1 + \frac{V}{\epsilon})$, while the HO background is not. Electron recoil signal should then appear as discrete peaks corresponding to $\mathrm{E}_{NTL} = N|eV|$ where $N$ is the number of electron-hole pairs, $e$ is the electron charge. For bias voltages such that $eV$ is significantly larger than the phonon sensor resolution, ERDM signals should form comb-like structure, differentiable from a smooth background of HO events.

The EDELWEISS collaboration achieved in 2020 a 46 eV resolution on a 33.6 g Ge prototype detector operated at 78 V [33], corresponding to a resolution of 0.53 electron-hole pair. While not sufficient to resolve individual values of charges, as achieved by the 1 g Si HVeV detector of Ref. [54], the low backgrounds attained by EDELWEISS resulted in more stringent constraints on ERDM signals. This confirmed for the first time the relevance of the use of relatively massive germanium detectors in the HV regime. Figure 4 (right panel) shows the event energy distribution following a $^{71}$Ge activation where we can clearly identify the X-ray lines from the electron-capture decays from the K/L/M shells at 10.37 keV, 1.3 keV, and 160 eV respectively. Thanks to this exquisite energy resolution, the collaboration has achieved the first Ge-based sub-100 MeV/c$^2$ dark matter search and the most stringent limit at the time on Dark Photons below $\sim 10$ eV/c$^2$ [33]. As can be observed from Fig. 4 (right panel), the HO excess is also clearly visible below 300 eV$_{ee}$. The latter has been found to dramatically reduce the dark matter search sensitivity of the RED30 detector prototype by several orders of magnitude. Following these results, the CRYOSEL program has started in order to design a cryogenic detector technology aiming for single-e/h detection combined with an active rejection of the HO excess background. The French TESSERACT partners will then develop few 10s of grams detector with sub-eV$_{ee}$ energy threshold and highly efficient HO discrimination to complement the ERDM reach of the TESSERACT experiment (see Sec. 5.2).

# 3 Experimental Apparatus at the Modane Underground Laboratory

In addition to the detector technology contribution, the French teams intend to provide access to the ideal environment for the ambitious science goals and intense cryogenic detector development program of TESSERACT. Exceptional low-radioactivity conditions and ease of access are key elements for its success.

The Modane Underground Laboratory (LSM) is a French national lab dedicated to the development of the astroparticle physics programme. Being protected from cosmic rays, it provides the low background conditions necessary for experiments dealing with rare or exotic interactions. It has been proven to be an ideal site for cryogenic searches for DM and for neutrinoless double-beta decay, as attested by the success of the EDELWEISS and CUPID-Mo programs.

The mean rock thickness of 1700 m (about 4800 m water equivalent) reduces the muon flux down to about 5 muons/m$^2$/d [55] , which is more than $10^6$ times smaller than at the surface. To further protect the TESSERACT detectors, this time from the surrounding rock radioactivity, they will be protected by passive shielding layers (see Sec. 3.1). Figure 5 shows the preliminary version of the planned layout of the Phase-1 crysotat (see Sec.1.2) of the TESSERACT experiment at LSM. The experimental setup, consisting of the cryogenics system, shielding, electronics, data acquisition along with the specialized ISO-6 clean room will be located in the previous EDELWEISS location. Utilities for the cryogenic system and radon suppression will be located on the mezzanine of the above mentioned area.

The cryostat of the future TESSERACT experiment at LSM will be either a Bluefors LD 400 or a CryoConcept HexaDry-UQT 200 which are both cryogen-free dilution refrigerator with 8 mK base temperature and allows for easy, integrated operations. Necessary laboratory services such as air conditioning, electrical power, cooling water, compressed air and network connections will be provided by LSM.

## 3.1 Shielding Design and Underground Integration

The shielding for TESSERACT is being designed based on early Monte Carlo simulations. They infer the acceptable contamination levels of the shielding materials along with their size. A sketch of the experimental set-up along with the shielding scheme is shown in Fig. 6.

The overall design of the TESSERACT shielding follows well-established techniques for reducing environmental backgrounds, using layers of hydrogenous material for neutron moderation and high-Z material to reduce the gamma flux. The final layer of shielding, closest to the detectors, must be of the highest radiopurity material. The outermost layer of the TESSERACT shield is composed of 15 cm of high density polyethylene (HDPE), which reduces radiogenic neutrons produced in the cavern walls. This first line of defense is called the outer neutron shield. The next layer inwards is a 20 cm-thick gamma shield made of lead which reduces the accompanying external gamma flux. This is followed by an additional layer of 27 cm polyethylene between the lead and the titanium outer vacuum can of the cryostat. This inner neutron shield attenuates any secondary neutrons from spallation, as well as neutrons and gammas emitted by trace internal radioactivity in either the cryostat or the lead. The “self-shielding” capability of the shield design, where each layer reduces the background flux from the outward layers, is a critical design feature. This enables a design in which only the innermost materials must be of exceedingly high purity, while the outer shielding layers can have looser purity restrictions, reducing costs for screening and assay. Part of the lead and polyethylene shielding for the TESSERACT LSM cryostat will be provided by the IN2P3 groups’s share of the available

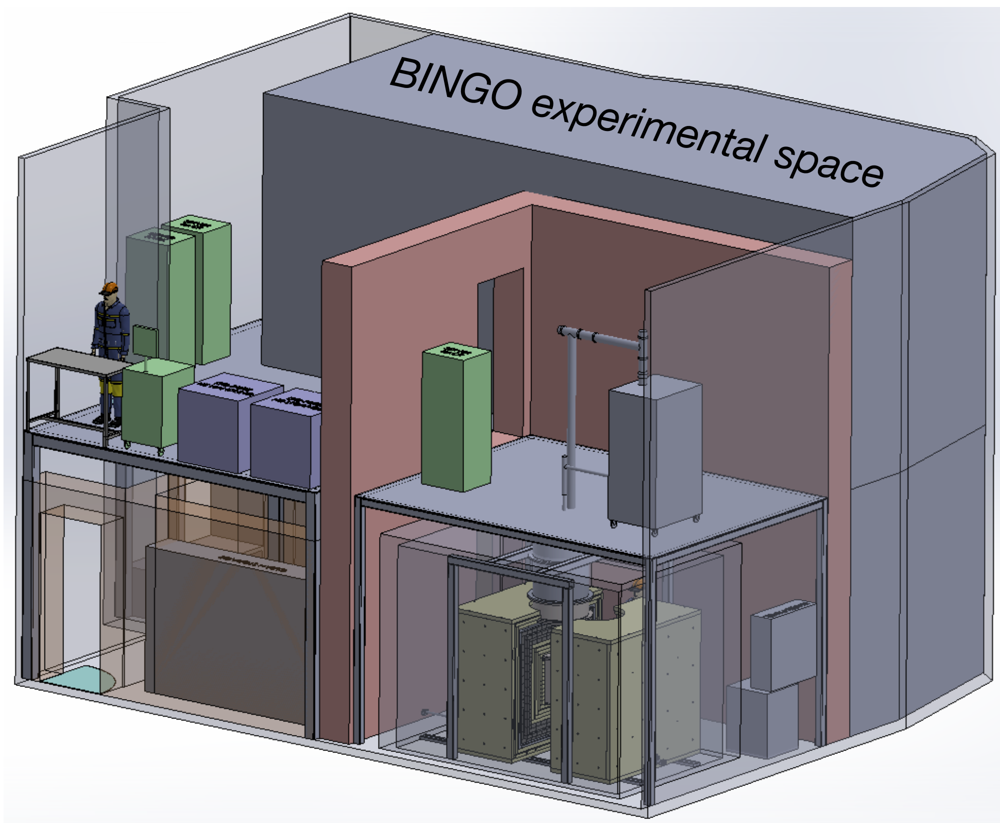


Figure 5: Proposed preliminary layout of the TESSERACT experiment at LSM - Phase I sharing the former EDELWEISS-III experimental space [56] with the BINGO $0\nu\beta\beta$ experiment [57].

material from EDELWEISS.

Protection from prompt radon gammas and prevention of radon daughter contamination over time necessitates a 5 cm-thick radon barrier layer outside the lead to maintain a nitrogen atmosphere within the shield interstices. A radiopure mu-metal shield between the inner neutron shield and the cryostat is also required in order to reduce the Earth's magnetic field at the detectors. Indeed, the phonon readout of TESSERACT detectors is based on SQUID amplifiers which performance (in particular their noise) is impacted by external magnetic fields. The required reduction of the external magnetic fields to a value close to $\sim$1 $\mu$T (at least a factor 50 below the Earth's value) will be achieved with a mu-metal cyclinder of $\sim$1 mm thickness around the external can of the cryostat.

The shielding is designed to be assembled from the bottom up and the outside inwards. All single pieces are small enough to be easily moved into the experimental hall either by hand, carts, or pallet jacks. Some parts such as the layers of the HDPE shielding might need to be pre-assembled. Similarly, we plan to perform steps such as cleaning and sealing the lead at suitable facilities at the surface to minimize risk and waste production underground.

## 3.2 Material and Assay Screening

All materials used to build the experiment as well as the detectors will be selected rigorously based on their high radiopurity level. The French groups intend to have a substantial contribution to the systematic campaign of radiopurity measurements of materials that will start in 2024 via alpha and gamma spectrometers. The gammas from the material bulk will be screened via HPGe detectors. The main detector will be **Gentiane HPGe**, currently operating at the LSM since 1997 and dedicated to the EDELWEISS experiment. It is an n-type HPGe diode of about 210 cm$^3$ mounted in a closed-ended coaxial configuration. Its sensitivity allows activity measurements down to the mBq level for U/Th chains.

A new dual HPGe detectors is under consideration to allow for higher efficiency measurements and gamma coincidence studies. The dual detector consists of **two Broad Energy Ge (BEGe) detectors** from Mirion. The BEGe detector covers the energy range of 3 keV to 3 MeV. The detector has a short, fat shape which greatly enhances the efficiency below 1 MeV for typical sample geometries. This shape is chosen for optimum efficiency for real samples in the energy range that is most important for routine gamma analysis. The BEGe detector also exhibits lower background than typical coaxial detectors because it is more transparent to high energy cosmogenic background radiation that permeates aboveground laboratories and to high energy gammas from naturally occurring radioisotopes such as $^{40}$K and $^{208}$Tl (thorium).

An **XIA UltraLo-1800** will be commissioned at a surface cleanroom at LPSC in the winter of 2024 to be moved underground at LSM. It will help with screening and assay of material surfaces.

The XIA Ultralo-1800 alpha particle counter is an ionization counter with a validated sensitivity of 0.0011$\pm$0.0003 alphas/cm$^2$/hr above ground. It can reach sensitivity as low as 0.0001 alphas/cm$^2$/hr when 700 m deep underground at Yangyang Underground Laboratory. The XIA has a drift chamber 15x21x21 inches in size which is filled with boil-off gas from a liquid argon dewar. The counting region is adjustable to a square region (1800 cm$^2$) or a circular region (707 cm$^2$), allowing non-destructive screening of large surfaces. Unlike proportional counters, using pulse shape analysis, the XIA counter is able to disentangle alpha particles originating on the sample tray from alpha particles originating on the chamber walls, ceiling or mid-air.

The XIA UltraLo-1800 detector is not fully dedicated to the TESSERACT screening campaign, and sample measurements will be requested and accorded on first come-first served basis following the LSM scientific priority. The dual HPGe detector will be procured to be dedicated to TESSERACT during the first years. An MoU with LSM will be detailed to secure smooth

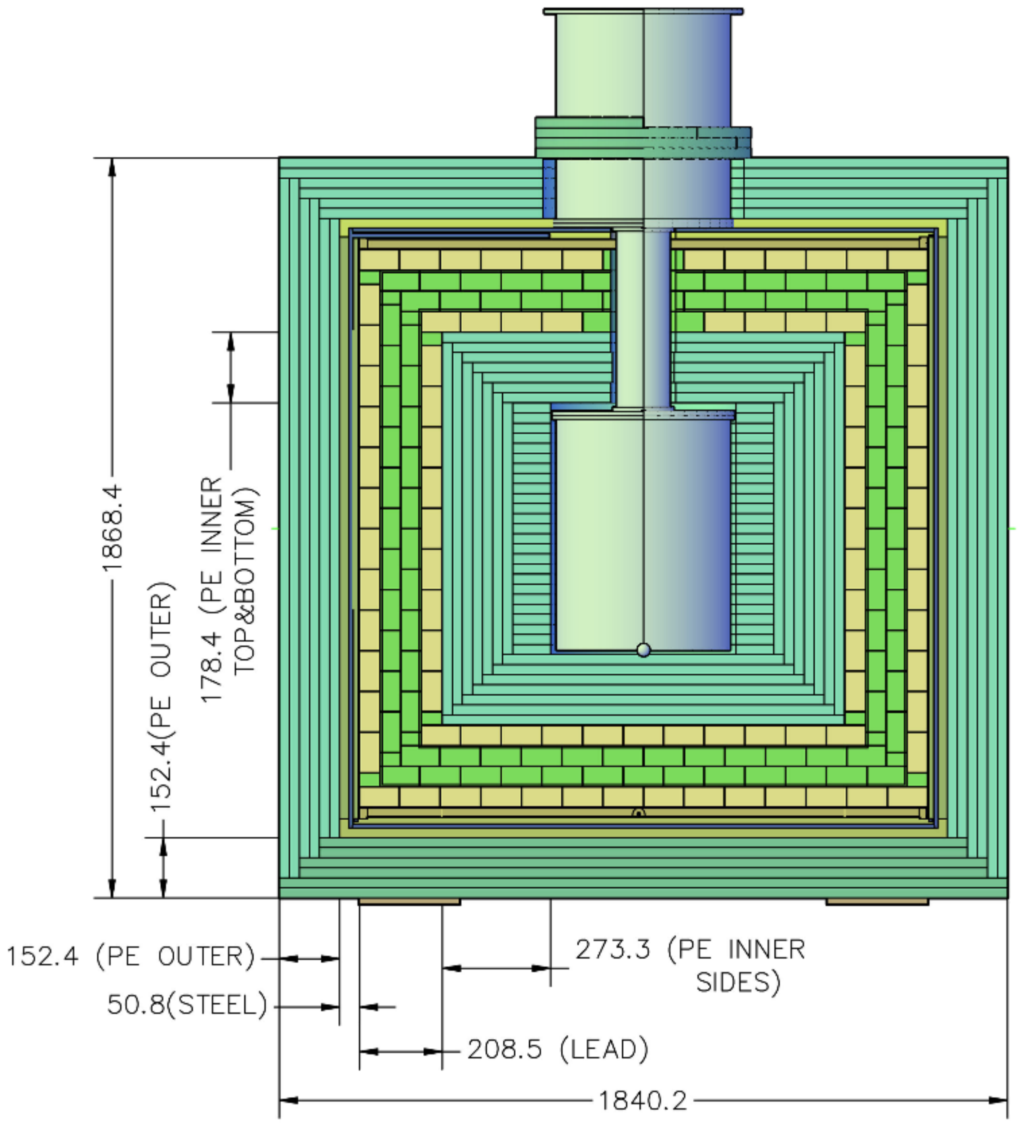


Figure 6: TESSERACT shielding with dimensions surrounding the central cryostat. We have, from outside to inside, a layer of PE, a stainless steel enclosure, lead bricks, another layer of PE, and then the cryostat. All measurements are in mm.

operations of the detectors underground and future uses, beyond the TESSERACT screening scope.

# 4 Radioactive Background Considerations

To achieve world-leading light dark matter sensitivities with TESSERACT, it is of the utmost importance to reach the lowest radioactive background levels. As discussed in this section, all sources are being considered and will be both assessed and minimized with both Geant4 simulations and extensive screening measurements. The overall targeted background levels of TESSERACT, before any detector rejection cuts, is about 5 evt/kg/keV/day for the gammas and less than $10^{-3}$ evt/kg/keV/day for the neutrons.

## 4.1 Radioactive sources

Among the different categories of background sources, we have identified eight sources that can generate undesired events in the detectors, potentially contributing background to the dark matter-candidate data set. These source categories are:

1 Coherent scattering of solar neutrinos on Ge nuclei (Coherent Neutrinos).

2 Radioactive impurities in the detector crystals (Detector Internal Contamination).

3 Radioactive impurities, particularly $^{238}$U and $^{232}$Th and their daughter products and $^{40}$K, uniformly contaminating the material of the detector hardware, cryostat and shield volumes (Material Internal Contamination).

4 Activation of other materials around the detectors by cosmic rays (Material Internal Activation)

5 Radioactive impurities contaminating the surfaces of all components (Surface Contamination). Surface sources are further sub-divided into two categories: those with and without a direct line of sight to the detectors. Only surfaces with direct line of sight (the detector faces and inner housing surfaces) produce detector-surface backgrounds (background source 9), while both categories produce detector-bulk backgrounds (background source 5).

6 Prompt radon decays in the interstitial air spaces within the detector shield (Prompt Interstitial Radon).

7 Radiation from the surrounding cavern environment (Cavern Environment).

8 Cosmic ray induced neutrons from the cavern wall or the shielding materials during experimental operations (In situ Cosmic Ray Induced Neutron Backgrounds).

9 Radioactive impurities contaminating the surfaces of the detectors or detector housings having line-of-sight to the detectors, particularly $^{210}$Pb from radon daughters (Surface Line-of-Sight Backgrounds).

The categories are defined by the methods by which they are estimated and/or mitigated. The cosmic ray induced neutron flux (source 8) is minimized by the underground location of the LSM. The design and implementation of the primary shield addresses the cavern and environmental backgrounds (source 7). Prompt radon decays in interstitial air (source 6) will be addressed by purging the shielding with a flow of dry nitrogen. A set of backgrounds (sources

2-5 & 9) will be minimized by a rigorous program of controlling material sourcing, production, shipping, cleaning, and assembly. Solar neutrinos (source 1) are an ultimately limiting background (producing the so called "neutrino floor or fog") for the currently envisioned experimental design. Surface background sources having line-of-sight to the detectors are assessed, studied, and mitigated in such a sufficiently different manner they are treated separately from the other background categories in most all background discussions to follow.

**Detector Internal Contamination -** The dominant backgrounds expected for the detectors are due to radioactive impurities within the detector crystals. The first measurement of the $^3$H decay rate in germanium detectors was done by EDELWEISS. It has been interpreted in terms of production rate of 82±21 nuclei/kg/day with statistical and systematic uncertainties combined [53]. That will require an excellent control of the detector exposure at surface and storage at shallow sites.

Indeed, exposure to high-energy cosmic-ray secondaries (i.e., neutrons, protons, and muons) results in the production of tritium ($^3$H) as a spallation product from interaction of the cosmic-ray secondaries with the nuclei in the detector crystals [58].

The long half-life of tritium ($t_{1/2}$=12.3 years) results in an accumulation of this radioactive impurity whose $\beta$-decay product has an endpoint energy of 18.6 keV. The tritium background will be modeled using a generic $\beta$-decay energy spectrum [59], the production rates, the activation times, and the detector crystal masses.

**Ge Activation Lines -** Exposure of the Ge detector substrates to high-energy cosmic-ray secondaries results in the production of several radioisotopes that decay by electron capture. Our background estimates will be based on the four isotopes measured in the EDELWEISS experiment [53] that are sufficiently long-lived to contribute background in the TESSERACT Ge detectors: $^{68}$Ge daughter, $^{65}$Zn, $^{55}$Fe and $^{49}$V. Each decay can proceed via electron capture from the K, L or M shell, giving rise to a total of 12 spectral peaks to be taken into account in the experiment background budget.

**Material Internal Contamination -** Radioactive impurities are introduced in all materials at some level during the manufacturing process. The $^{238}$U and $^{232}$Th isotopes are unstable but long-lived and are present in most materials at low concentrations. Both of these isotopes have a chain of decay daughters that are assumed to be in secular equilibrium. Additionally, isotopes such as 40K and 60Co are naturally present in many materials because of their long half-lives, but they do not have accompanying series of daughter radioisotopes. The TESSERACT groups at LPSC and IP2I Lyon have focused and will expand assay efforts on those materials and components that are either unique to the TESSERACT experiment or are of particular concern due to their relative contribution to the background prediction.

**Material Internal Activation -** Exposure to high-energy cosmic-ray secondaries results in the production of long-lived radioisotopes in the construction materials surrounding the detectors. In particular, the cosmogenic activation of copper presents a background source for the TESSERACT experiment. Copper is used both for the detector mechanical assembly and support and the nested cylindrical cryostat canisters.

**Surface Contamination -** Materials accumulate concentrations of radioactive isotopes on surfaces exposed to air containing dust and radon. Airborne dust typically contains relatively high concentrations of $^{238}$U, $^{232}$Th, and $^{40}$K. Daughters from the decay in air of $^{222}$Rn may implant shallowly into a material surface, resulting in a buildup of the long-lived $^{210}$Pb that later decays through a short chain and produces a roughly constant emission rate of X-rays, betas and alphas.

The detector response and detector type are particularly important considerations when evaluating the impact of the surface backgrounds on the experimental sensitivity. Building up on the successful experience from the EDELWEISS-III collaboration in measuring and disentangle the surface events via the FID technology [52], the French teams are the best suited experts in the field. The order-of-magnitude improvement in ionisation resolution achieved by RICOCHET promises an outstanding discrimination power against surface events and optimal conditions for a thorough test of the stringent cleaning and dust exposure protocols that will be developed for the detector installation.

**Prompt Interstitial Radon** - Radon decays in the underground laboratory air produce moderately high-energy gamma-rays via the $^{214}$Pb and $^{214}$Bi daughters. We assume a radon level of 15 Bq/m$^3$ in the LSM underground laboratory based on a measurement performed by EDELWEISS [60]. EDELWEISS has also shown that this background can be reduced by three orders of magnitude by sealing the region between the lead gamma shield and the cryostat and purging it with a flux of de-radonized air. Such seal was achieved without transmitting environmental vibrations from the shield to the cryostat.

These classes of backgrounds provide a list of sources to investigate, many of which are amenable to quantification using the GEANT4 Monte Carlo code developed by the collaboration for radiation transport package. For each component volume in the GEANT4 framework, we create multiple source datasets by distributing radioactive nuclei (in particular $^{238}$U, $^{232}$Th, $^{40}$K, and cosmogenically activated isotopes) or equilibrium neutron spectra uniformly over the surfaces or throughout the volume. The resulting simulation output files are then analyzed in a post-processing stage to determine the fraction of background source generated primaries result in a energy deposition in a detector crystal. Each component in the experiment's bill of materials is associated with a single GEANT4 volume, and the appropriate simulation dataset is used to calculate background rate for any given background source. Where the required CPU time is not prohibitive, in particular for all of the detector and housing components, a proper statistic to simulate is equivalent to 50 years of decays for each volume. For small or very thin components such as readout cables and printed circuit boards, we do not distinguish between surface and bulk sources in simulation.

The French collaborators have a recognized expertise in the simulation of all these backgrounds (acquired notably in the EDELWEISS and RICOCHET experiments) and plan to contribute strongly to these efforts, using the available tools and resources at the IN2P3 Centre de Calcul.

## 4.2 Total radioactive background budget

The initial simulations performed by TESSERACT are based on the rock composition and density of the Homestake formation. A statistic of $10^{10}$ external $\gamma$-rays from $^{238}$U and $^{232}$Th chains and about $10^9$ neutron events from ($\alpha$,n) and spontaneous fission in cavern walls were simulated. Internal backgrounds of the shielding material are modeled using measured radioactive activities in titanium, stainless steel, copper, and polyethylene as published by SuperCDMS, EDELWEISS, LZ and other experiments.

Extensive simulations of the entire TESSERACT installation as planned for LSM will be required in order to finalize the selection of the construction materials and optimize the passive shielding design, satisfy the background requirements, and set limits on the amount of cosmic ray exposure. The final design must achieve backgrounds sufficiently low to meet the science goals of the experiment.

In order to achieve the science goals of TESSERACT, the radioactive background of the facility (underground environment, shielding, cryostat and detector components) has to be $<$ 10 evts/kg/keV/day (DRU) below 1 keV before any detector discrimination power. The CUTE underground test facility [61] at SNOLAB has proven a radioactive background budget validated in a 600 g Ge detector of 6.7$\pm$0.8 evts/keV/kg/day in the energy range from 1 to 1000 keV from all facility components [62]. About 10% of the rate is contributed by the detector stack. The major contributors to the background budget are the gammas from the SNOLAB cavern ($\sim$30%), the inner layer of the external lead shield ($\sim$20%) and the stainless steel of the OVC ($\sim$13%).

Most of the external gammas enter through the gaps between the external and internal lead shielding. If a lower background budget is required for TESSERACT, we would pay attention to it during the shield design study considering additional gamma shielding to reduce those gaps, and replacing the highest contributors from the facility (TFA lead shield and OVC) with lower activity materials (lower activity lead for the shield for instance). For the OVC, TESSERACT is indeed considering clean radiopure titanium material from LZ experiment. Lastly, specifically designed cryogenic detectors acting as active veto, as planned by the BINGO [57] and NuCLEUS [63] experiments, could be used to further reduce the TESSERACT background levels if needed.

# 5 Proposed French Detector Technology and Science Reach for TESSERACT

In this section we detail the proposed French detector technology contribution for the TESSERACT experiment at LSM and its science reach. As described in Sec. 2.5, our plan is to focus on both ERDM and NRDM searches with optimized semiconducting cryogenic detectors, which builds upon the legacy of the former EDELWEISS experiment and today's Ricochet and CRYOSEL programs, and also benefits from synergetic developments with CUPID. For now our focus is on using Ge target material, given its excellent performance and our expertise, but complimentary targets such as Si and diamond will be investigated at later stages.

## 5.1 NRDM searches with low-voltage semiconducting detectors

**Existing detector performance** – Following the successful completion of the EDELWEISS scientific program, which has pioneered the dual readout of phonon and ionization energies at the few keV-scale for $\mathcal{O}(10)$ GeV DM particle mass, the Ricochet collaboration has taken the lead in pushing the "low voltage" cryogenic Ge technology down to the $\mathcal{O}(100)$ eV energy scale. Indeed, the Ricochet experiment aims at measuring with high precision the reactor neutrino induced nuclear recoils via the Coherent Elastic Neutrino Nucleus Scattering (CENNS) process down to 100 eV to search for new physics in the electroweak sector [64]. To do so, the French IN2P3 Ricochet team, which encompasses the French TESSERACT team, is currently developing the next generation of "low-voltage" Ge cryogenic detectors, called CryoCube, designed to reach $\sigma_{\mathrm{ion}} = 20$ eV$_{ee}$ and $\sigma_{\mathrm{ph}} = 20$ eV baseline energy resolution (RMS) in ionization and phonon energies, respectively, with a total payload of 1 kg of Ge target material [65].

Figure 7 (left panel) is a photo of a sub-array of the CryoCube, called MiniCryoCube, which can host up to three 42 g Ge crystal detectors equipped with an NTD (Neutron Transmutation Dopped) heat sensor and aluminum electrodes to simultaneously measure both the phonon and ionization energies following a particle interaction. The MiniCryoCube is made of two stages, a 10 mK stage hosting the three detectors and a 1 K stage hosting the front-end HEMT-based electronics for the ionization readout[4]. In June 2023 the Ricochet collaboration successfully achieved an unprecedented ionization resolution of $\sigma_{\mathrm{ion}} = 30$ eV$_{ee}$ (RMS) with a common source preamplifier topology, commercial amplifiers and filters at room temperature [67]. This result was the first demonstration that such performance was achievable with bolometers operated at

[4]The High Electron Mobility Transistors (HEMT) used in our work are developed by the Center for Nanoscience and Nanotechnology (C2N) and commercialized by CryoHEMT [66].

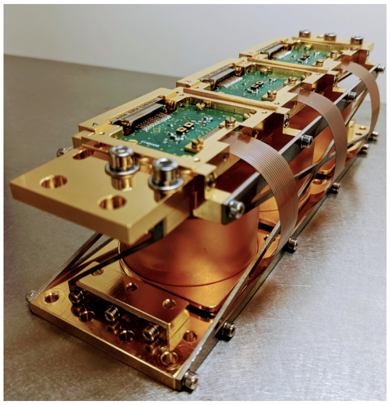

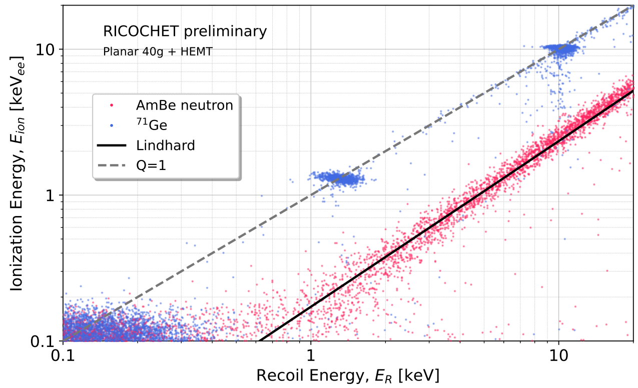


Figure 7: **Left:** Photo of a MiniCryoCube assembly, hosting the detectors RED127, RED167, and RED237 (from left to right), with its two stages at 10 mK hosting the three detectors, and at 1 K hosting the HEMT-based electronics. **Right:** Event distribution in the ionization versus recoil energy plane obtained with RED167 from the Ricochet collaboration operated at IP2I in a MiniCryoCube detector array. The blue dots correspond to "low background" data with the K- and L-shell X-ray lines clearly visible, and the red dots correspond to neutron calibration data. Note that the large population of events below $E_{\text{ion}} = 160$ eV$_{ee}$ and $E_R = 400$ eV corresponds to the so-called "noise-blob". Note the tremendous detector improvement between the EDELWEISS-III (Fig. 4 – left panel) and Ricochet low-voltage detector technologies.

15 mK and represents an improvement by a factor of 7 and 11 with respect to previous resolutions achieved by the EDELWEISS and SuperCDMS collaborations, respectively. Nowadays, the Ricochet French team is testing its newly designed room temperature electronics that allows for a dual measurement of phonon and ionization energies [68]. First results obtained in July 2023 are shown in Fig. 7 (right panel) where we show the event distributions in the ionization versus recoil energy plane from "low background data" (blue points), where we can clearly see the K- and L-shell lines at 1.3 and 10.37 keV, and from an AmBe neutron calibration data (red points). The performance obtained then were about 44 eV$_{ee}$ and 60 eV baseline resolutions (RMS) for the ionization and phonon energies, respectively. Though still a factor of 2-to-3 from the CryoCube specifications, this result has tremendous implications as it demonstrates for the first time 1) the viability of the CryoCube technology, and 2) that particle identification can be extended well into the sub-keV energy region as required for Ricochet , see Fig. 4 (left panel) for comparison with former EDELWEISS performance. It is worth highlighting that the CryoCube detector technology developed in the context of Ricochet is particularly relevant for TESSERACT. Indeed, CENNS kinematics from reactor neutrino is very similar to that of a DM particle with a mass of about 2.7 GeV. As such, the CryoCube detector is specifically designed to detect, and identify over the radioactive and "Heat-Only" backgrounds, a putative DM signal with a mass of 2.7 GeV and above. Searching for lower DM masses will therefore require 1) a reduced phonon energy threshold and ionization energy resolution, 2) a reduction of the overwhelming "Heat-Only" background, and 3) a dedicated ultra-low background setup underground as planned for the TESSERACT experiment, see Sec. 3.

**Detector performance milestones and subsequent science reach** – The goal of the "low voltage" semiconducting cryogenic bolometer program is to achieve unprecedented NRDM

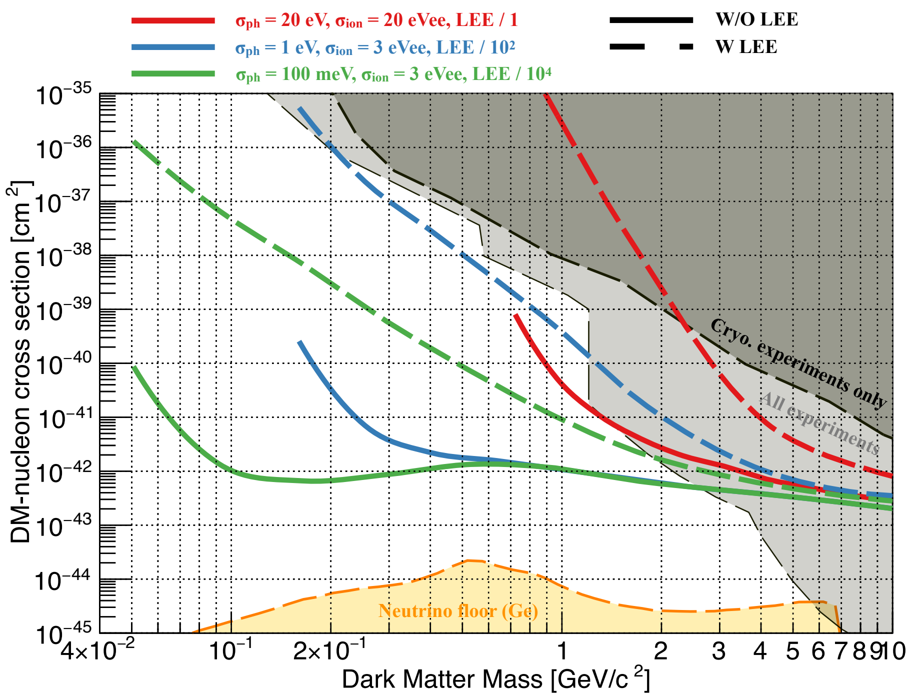


Figure 8: NRDM sensitivity projections of three detector configurations in the dark matter and cross section plane for a constant payload of 100 g.year : (dashed red line) 20 eV phonon, 20 eV$_{ee}$ ionization, no reduction of "heat only"; (dashed blue line) 1 eV phonon, 3 eV$_{ee}$ ionization, reduction of "heat only" by 100; (green dashed line) 100 meV phonon, 3 eV$_{ee}$ ionization, reduction of "heat only" by $10^4$. "Heat only" background free sensitivities are also shown as the red, blue, and green solid lines. The orange, gray and dark gray contours are the so-called neutrino floor [69, 70], the existing exclusions from all experiments, and the ones only from the cryogenic experiments, respectively.

sensitivities down to 50 MeV DM mass with highly efficient particle identification and background rejection capabilities, against bulk and surface backgrounds, and against the overwhelming "Heat-Only" excess. To achieve this scientific goal, and based upon the charge and phonon readout developments from RICOCHET and the athermal TES from TESSERACT (see Sec. 2.1), we propose to develop 1 cm$^3$ crystal targets with ultimate 3 eV$_{ee}$ and 100 meV ionization and phonon baseline energy resolutions (RMS), respectively. Regarding the ionization performance, a new electrode design, combined with a new crystal holder strategy, will be developed in order to achieve a detector capacitance of 1 pF with negligible parasitic capacitance. Our HEMT-based preamplifier model suggests that with a 2 pF total capacitance (detector + HEMT) we could achieve single-electron charge resolution readout [71]. On the phonon resolution side, we plan to switch from the currently used NTD to the more sensitive athermal phonon TES sensors discussed in Sec. 2.1. Additionally, ongoing work, from our US partners, studying the low energy excess background with the TES sensors from TESSERACT seem to suggest that a significant fraction of the "Heat-Only" events are coming from the sensor itself. In depth studies are ongoing to reduce the TES film induced stress in order to dramatically reduce this overwhelming and particularly damaging background.

Figure 8 illustrates NRDM sensitivity projections from a 100 g-yr Ge "low-voltage" detector payload operated at a voltage bias of 4 V. We consider here three sets of detector performance milestones, starting from the almost existing MiniCryoCube technology from Ricochet (red lines) to our targeted ultimate performance (green lines). We then subdivided the sensitivity projections into two categories: without including the LEE in the background model (solid lines), and including the LEE (or "heat only" background) with varying intensities following reasonable assumptions (dashed lines). Sensitivities have been computed using the radiogenic background from Sec. 4.2, including the overwhelming "Heat-Only" background as measured by the RED20 [32] and RED30 [33] EDELWEISS prototype detectors, and the boosted decision tree analysis from [72] without background subtraction. For the dashed lines, the first reduction of the "heat only" rate by a factor 100 (blue dashed line) is justified by switching from NTD to TES. Indeed, EDELWEISS detectors using NTD have been documented to have a LEE about 100 times larger than the ones from CRESST-III using similar crystal masses but with TES [73], possibly due to the use of glue [74]. The following reduction by a factor of 100 (green dashed line) is motivated by the ongoing work on stress induced films currently being carried out by the TESSERACT US partners.

As one can see from Fig. 8, first leading NRDM results are to be expected on a short timescale with a single Ricochet MiniCryoCube detector array for a DM particle mass of 3 GeV and above, thanks to its $\mathcal{O}(100)$ eV energy scale particle identification capability. The blue and green projected sensitivities correspond to what we expect after switching to athermal TES, leading to both improved phonon baseline energy resolutions and reduced HO background, and achieving single-e/h pair charge resolution hence extending our particle identification capabilities down to the $\mathcal{O}(10)$ eV energy scale. Figure 8 also presents projected sensitivities without including the HO background, shown as solid red, blue, and green lines, in order to appreciate what would be the ultimate NRDM reach of our technology assuming that the low energy excess is both fully understood and mitigated in the coming years. Lastly, Fig. 8 shows that, even with moderate payloads of 100 g.year and despite of the presently observed low energy excess (HO), our low-voltage semiconducting cryogenic bolometer program will allow to achieve world leading NRDM sensitivities down to a DM particle mass of 50 MeV over the next few years. It is also worth emphasizing that only such cryogenic detectors, directly measuring the nuclear recoil energy, can probe such sub-GeV DM particle masses with minimal systematic uncertainties. Larger payloads in the 1 kg.year scale, or above, are also envisioned in a longer time scale and would be compatible with the TESSERACT low-background setup at LSM.

Lastly, it is worth highlighting that this program is complementary to the NRDM searches with HeRALD as it uses different target nuclei (germanium at first, and possibly silicon and diamond later on) and different detection techniques which are both pushing for particle identification and efficient rejection of the low-energy excess.

### 5.2 ERDM searches with high-voltage semiconducting detectors

**The CRYOSEL detector development program** – The CRYOSEL proposes a high-risk, high-reward high-voltage alternative technology to complement the more gradual path towards low threshold offered by the low-voltage CryoCube program. The CRYOSEL strategy focuses more aggressively on the rejection of HO background in searches involving signal comprising one or a few electrons, a problem that is central in the case of ERDM searches [33]. Indeed, the ERDM searches performed with the 33 g detector of Ref. [33] were by far more limited by this background than by the energy resolution or the leakage current. The CRYOSEL strategy was encouraged by the possibility to reduce the HO background in an EDELWEISS detector equipped with thin-film NbSi TES sensors that were capable to measure the spatial dependence of athermal phonons [75], [76].

In the CRYOSEL design, the charge electrode readout is replaced by a very sensitive athermal phonon sensor, detecting the large flux of phonons emitted via the NTL amplification process when charges drift through a small, very high electric field region. This specific field configuration is achieved by using the phonon sensor itself as a point-contact like electrode, as shown in Fig. 9. A NbSi layer deposited on the crystal surface is patterned to a 10 $\mu$m circular line having a diameter of 2 to 5 mm. The NbSi film can operate either as a TES or in a proposed innovative regime called SSED (Superconducting Single Electron Device) well below its critical temperature. At high charge-collecting voltage the SSED is expected to trigger on single electron-hole events and tag the presence of charge. While phonons emitted by HO events may be expected to be distributed uniformly over the entire crystal volume, nearly all NTL phonons are emitted in a few mm$^3$ zone located under the NbSi microwire phonon sensor. In these conditions a suppression factor >1000 of the HO event rate is expected . The SSED design will be optimized to trigger on single-charge events but is not expected to read the charge signal with a high resolution. A high-resolution measurement will be provided by a NTD-Ge thermistor glued on the Al electrode. A 20 eV NTD phonon resolution and a bias of 200 V is sufficient to provide a <10% resolution on the peaks due to the detection of discrete number of electron-hole pairs. ERDM signals should thus correspond to discrete Gaussian peaks over the smooth HO background spectrum, strongly suppressed by the SSED rejection efficiency.

The CRYOSEL R&D program has started in 2021, and has the support of an ANR since 2022. The ANR objectives focus on the determination of the rejection power for HO events, on the SSED response to surface and incomplete charge collection events, and on the strategy to limit dark current events. This ANR program will be concluded by the end of 2024, with the planned operation of a single SSED detector for a few months in the BINGO cryostat in order to perform a 1 kg·day exposure test of the technology in an underground environment.

Furthermore, we remark that the Ge detectors operated in Trofimov-Neganov-Luke high-voltage mode correspond to the solution that the double beta decay experiment CUPID has selected for the light detector technology of their scintillating bolometers. TESSERACT and CUPID can thus benefit from a mutually fruitful interaction, especially regarding the construction of this type of detectors at IJCLab, helping to address common technological and manufacturing challenges.

**Achieved milestones** – The CRYOSEL ANR project has already achieved its primary goal of establishing that this original method to tag charges using NTL phonons does indeed work. A first full operational 35 g prototype (CRYO50) has been tested at IJCLab and IP2I. In addition to being equipped with a NTD and a SSED, it had a charge amplifier readout in the enveloping aluminum electrode in order to cross-check the SSED response. Figure 9 bottom right shows the ionisation versus phonon signals collected at a bias of 60 V while the detector is at 15 mK, well below the superconducting-to-normal transition of the NbSi film ($T_c$ = 47 mK). The black dots are events where a pulse is observed on the SSED, in coincidence with the NTD and electrode signals, while no such pulses were observed for the red dots. The 1.3 and 10.37 keV$_{ee}$ electron-recoil events are systematically tagged by the SSED, while the HO events above 1 keV (along the horizontal axis) are systematically rejected by the SSED tag. This proves that the concept of charge tagging using NTL phonons with a SSED is sound.

The ANR developments are now in the process of reducing the thresholds of the SSED and NTD, with tests on a recently produced prototype having just been started. Better performance requires reducing the $T_c$ (a reduction from 47 to 35 mK has already been achieved in the last prototype), improving the phonon collection efficiency (via a design reducing the amount of Al close to the sensor and an increase of the NbSi film thickness), increasing the maximum bias

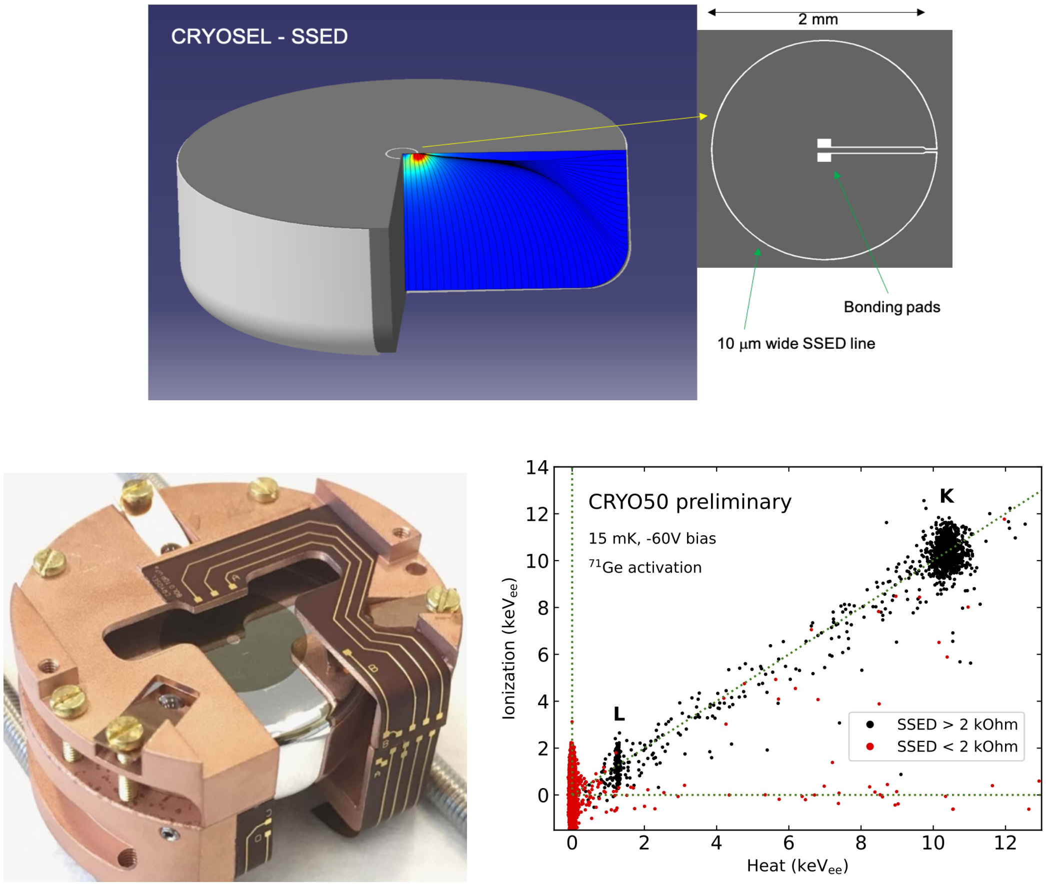


Figure 9: Top: General geometry of a CRYOSEL detector. The dark grey is the germanium crystal. The light grey is the enveloping aluminum electrode. The white circle on the top is a circular NbSi microwire that acts both as phonon sensor and as counterelectrode. The resulting field lines are strongly focused in a small high-field region (in red) just facing the microwire. Bottom left: picture of the first CRYOSEL prototype. Bottom right: ionisation versus phonon signals recorded following its $^{71}$Ge activation, and at an operating temperature of 15 mK. The red (black) points correspond to events in coincidence (anticoincidence) with a pulse on the SSED sensor.

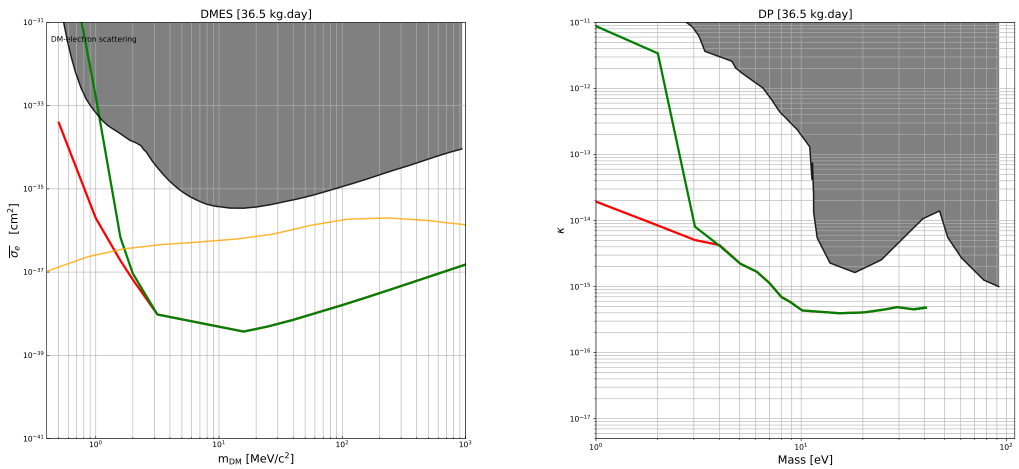


Figure 10: ERDM sensitivity projections of two detector configurations for a constant payload of 100 g.year : (green) 20 eV phonon, 200 V, reduction of "heat only" by 1000 starting at a threshold of 2 electron-hole pairs; (red) 20 eV phonon, 200 V, reduction of "heat only" by 1000 starting at a threshold of 1 electron-hole pairs. The gray contours are the existing exclusions.

that can be applied (the new prototype can sustain a bias of 150 V thanks to an optimized design of the layers deposited under the electrodes), and improving the sensitivity of the NTD.

**Future milestones and subsequent science reach** – This intense program should rapidly provide the two orders of magnitude improvement on the energy threshold needed to obtain discrimination at the single-electron level. In addition, the ability to compare charge, thermal and athermal signals in coincidence will soon provide information on the nature and origin of the HO background that will be very useful in optimizing future CRYOSEL and CryoCube designs. In particular, the shape of spectrum in the single-electron peak range will help determine the nature of the leakage current, as surface currents and detrapping should not produce peaks with discrete number of electron-hole pairs. The wealth of information provided by the CRYOSEL readout and the possibility to study the detector response as a function of the applied bias and the temperature of operation should provide innovative techniques to evaluate and control charge de-trapping effects and leakage current mechanisms that are essential to probe single-electron signals.

Figure 10 shows the limits that can be achieved with a 100 g·year exposure with an array of CRYOSEL detectors with a NTD resolution of 20 eV and a bias of 200 V and a factor 1000 HO background suppression. Two cases are considered whether the leakage currents prevent the use of the one-electron peak or not. Even in the worst case, a CRYOSEL array is clearly an attractive payload for the TESSERACT Phase-1 cryostat at LSM.

The planning of a second detector phase with single-electron trigger depends on the device sensitivity to backgrounds from surface and dark current events. The best strategy will be either to maximize the phonon resolution by reducing the detector unit mass and/or by developing a high-performance TES suited for CRYOSEL operations, or to use the largest possible detector unit mass and detector bias compatible with a sub-electron resolution. If needed, the EDELWEISS-III detectors, stored at LSM since 2013, are an available source of large Ge crystals with reduced tritium content. The advancement toward the ideal zero-background sensitivity will largely depend on the progress in understanding the nature and phenomenology of the new backgrounds that will be encountered in this low energy domain.

## 5.3 Low energy ER and NR calibrations

**Calibration requirements -** The calibration of the detectors used in the search for low-energy DM particles is particularly challenging. The energy range from 1 eV to 1 keV correspond to photons and X-rays that are absorbed in the first $\mu$m of the surface, and may be not representative of the response to energy deposits in the bulk. The response to nuclear recoil in the bulk may be studied using neutron scattering, but monochromatic neutron beams are difficult to achieve, and produce wideband recoil energy spectra.

At high energy, the ionisation response of a semiconductor can be simply described by an average energy needed to create one electron-hole pair ($\epsilon$ = 3 eV in Ge) and a Fano factor [77] describing the Gaussian fluctuations around this average value. This simple behavior breaks down in the low energy domain relevant for TESSERACT. Below 10 eV$_{ee}$, these fluctuations are no longer Gaussian [78]. For low-voltage detectors, the effect of charge recombination and trapping are of concern; high-voltage detectors also have to contend with impact ionisation effects. The gain of the ionisation channel must be monitored as a function of time, as trapped charges are accumulated.

Nuclear recoil events have the added complication that the their ionization yield is reduced by an energy-dependent quenching factor $Q$ relative to electron recoils. The atomic approximations on which is based the Lindhard theory [79] describing this effect are expected to break down at low energy.

An important asset of cryogenic detector is that, to first order, the thermal signal from an NTD sensor and to some extent the ballistic phonon signal from a TES should be insensitive to the origin of energy deposition process. However, a few percent of the energy from nuclear recoils is expected to be stored as defects in the crystal, resulting in a measured quenching factor $Q'$ for heat and phonon signals. Available measurements in Ge are in the 0.91–0.94 range, with significant systematic uncertainties [80, 81].

One of the advantage of using germanium target in TESSERACT is that the properties of this material allows a wide array of techniques that covers all the needs to determine precisely and comprehensively its low energy calibration for both electron and nuclear recoils.

**Calibration by neutron activation -** The absolute energy calibration is greatly simplified by the possibility to activate the crystal with thermal neutrons. The absorption of thermal neutrons by $^{70}$Ge produce the isotope $^{71}$Ge, with a period of 11 days. The subsequent decays by electron capture in the K, L, and M shells produce deexcitation lines at 10.37, 1.30, and 0.16 keV, respectively (see Fig. 4). The $^{71}$Ge atoms are produced uniformly in the entire detector volume, and the emitted X rays have mean free paths below 40 $\mu$m and are thus locally absorbed, thus providing very good probes of the detector response to a DM signal. The activation can be done weeks before the detector is cooled down [33], or at any time if the experimental setup can accommodate a night exposure with an intense AmBe source [75]. In addition, the $L/K$ and $M/L$ yields are known with precision [82, 83], allowing a direct measurement of the dependence of the efficiency as a function of energy. The study of large and relatively pure sample of $K - shell$ events makes possible detailed studies of the tails of the distribution of the response of the detector, as shown in Ref. [76].

**Laser calibration of electron recoils -** The response to electron recoils in the 0.7 to 160 eV range is calibrated using pulses from an infrared laser. This technique is well demonstrated in Ref. [84]. The pulsed light of a room-temperature laser is introduced inside the cryostat via optical fibers carefully thermalised at each temperature stage, and mounted as to illuminate directly the detector inside its IR-tight copper casing. The choice of calibrating either bulk or

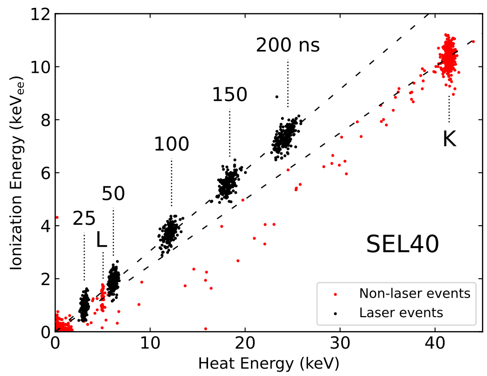


Figure 11: Ionisation and phonon signal obtained in a 3.3 g Ge detector [84] activated in $^{71}$Ge and exposed to pulses from a 1550 nm laser of varying lengths (25 to 200 ns). The black (red) dots correspond to events in coincidence (anticoincidence) with the laser pulses.

surface events is controlled by the precise choice of the laser wavelength. This technique is an efficient way to probe the response of the detector for the ionisation and phonon signal at any arbitrary energy, using the pulse width to vary precisely the average number of IR photon per burst. The TTL signal accompanying each laser burst provide a tag that makes possible to measure absolute efficiencies even at energies below the detection threshold.

**Calibration of nuclear recoils -** One major advantage of phonon-and-ionization detector is the event-by-event measurement of both the total energy deposited in the detector and the ionization yield. The expected ionization yield as a function of energy for nuclear recoils can be readily obtained by exposing the detector to a flux of fast neutrons. Many such measurements have been performed in EDELWEISS [51], using a standard AmBe or $^{252}$Cf source. The improved phonon and ionization of the RICOCHET detector has made possible the extension of these measurements to record low energies (Fig. 7).

Reaching a precision at the percent level on the energy scale requires to complement this data with a precise measurement of the fraction of energy lost to permanent defects in atomic collisions (e.g. see Ref. [80]). Members of the TESSERACT collaboration have developed a monoenergetic source of 24 keV neutron [85] using a $^{124}$S$^{9}$Be source and a iron filter. Using this source, and tagging the scattered neutrons with a liquid scintillator such as the one used in Ref. [85], it would be possible to probe in detail the response to germanium recoils with kinetic energies between 0.3 and 1.0 keV. In Ref. [86], it was noted by the CRAB collaboration that one of the final state of the thermal neutron absorption by $^{74}$Ge was a 300 eV nuclear recoil in coincidence with an energetic gamma-ray line that can be used as a tag. Contact have been made with the CRAB collaboration to provide a RICOCHET detector suited for a precise measurement of both $Q$ and $Q'$ at that energy, similar to the recent successful measurement [87] of 112 eV tungsten recoils in a cryogenic detector.

The main challenge with a $^{124}$S$^{9}$Be or CRAB calibration is that an high event rate is needed to ensure a good signal-to-noise ratio. Replacing the NTD by a faster TESSERACT TES would reduce the dead-time by more than two orders of magnitude, and ensure the succes of these experiments.

# 6 Tesseract WBS

The WBS structure currently in place for TESSERACT was developed by the TESSERACT DOE new initiative project and is detailed here below. It consists of mainly DOE-based institutions. We are discussing additional items to be included in the WBS for which the french groups will take responsibilities. Among them, we highlight Level-1 responsibility for the experimental apparatus integration underground at LSM and Level-2 responsibilities under the "Backgrounds" and "Semiconductor Detector" along with the RICOCHET MiniCryoCube initial readout and the HEMTs technology. The top, Level-1 WBS items are detailed below. The schematic structure along with the responsibilities per WBS item are shown in Fig.12. Blue color boxes refer to DOE-institute responsibilities and green color boxes to French institutes and universities.

1.1 Project Management and Integration
1.2 Sensors and Crystals
1.3 Helium Detector
1.4 SPICE Detector
1.5 Semiconductor Detector
1.6 Calibrations
1.7 Cryogenics
1.8 Shielding and Veto
1.9 Backgrounds

Most tasks will be shared among US and French laboratories, with significant overlap and collaborations. Depending on the allocation of resources that will be decided by the directions of their respective laboratories, the French group are proposing to take the lead in the following tasks:

**Project Management and Integration: Test Facility at IP2I Lyon**: coordinated by IP2I as it will involve its CRYORED low-background cryogenic test facility, but most tests will require a strong collaborations with the LPSC and IJCLab groups to build on the expertise gained in the operation of EDELWEISS and RICOCHET detectors.

**Project Management and Integration: LSM Site** : the LPSC group intends to have a leading role in the underground integration of the TESSERACT experiment, while the IP2I and IJCLab will bring their EDELWEISS expertise.

**Sensors and Crystals: HEMT Development** : IP2I would continue to coordinate this activity started in the context of the RICOCHET collaboration.

**Semiconductor Detector: Fabrication**: The IJCLab cryogenic detector fabrication facility will be the main infrastructure for the realization of the TESSERACT semiconductor devices. This task will be coordinated by IJCLab, and benefit from its extensive expertise in solid state detector and sensor physics. Strong collaboration is planned between the TESSERACT groups for the development of the future "low voltage" detector, in order to combine the single-charge HEMT read-out design with the athermal phonon sub-eV threshold TES, proposed and manufactured respectively by the French and US teams. The "high voltage" and "low voltage" detector prototypes will be systematically tested and optimized at the IJCLab and IP2I cryogenic test facilities.

**Semiconductor Detector: Detector Support and Interface**: IP2I intends to coordinate this task as in RICOCHET . This integration work, crucial for detector performance, involves the mitigation of vibrations and microphonics as well as the optimisation of the very-front-end electronics in the sub-K environment.

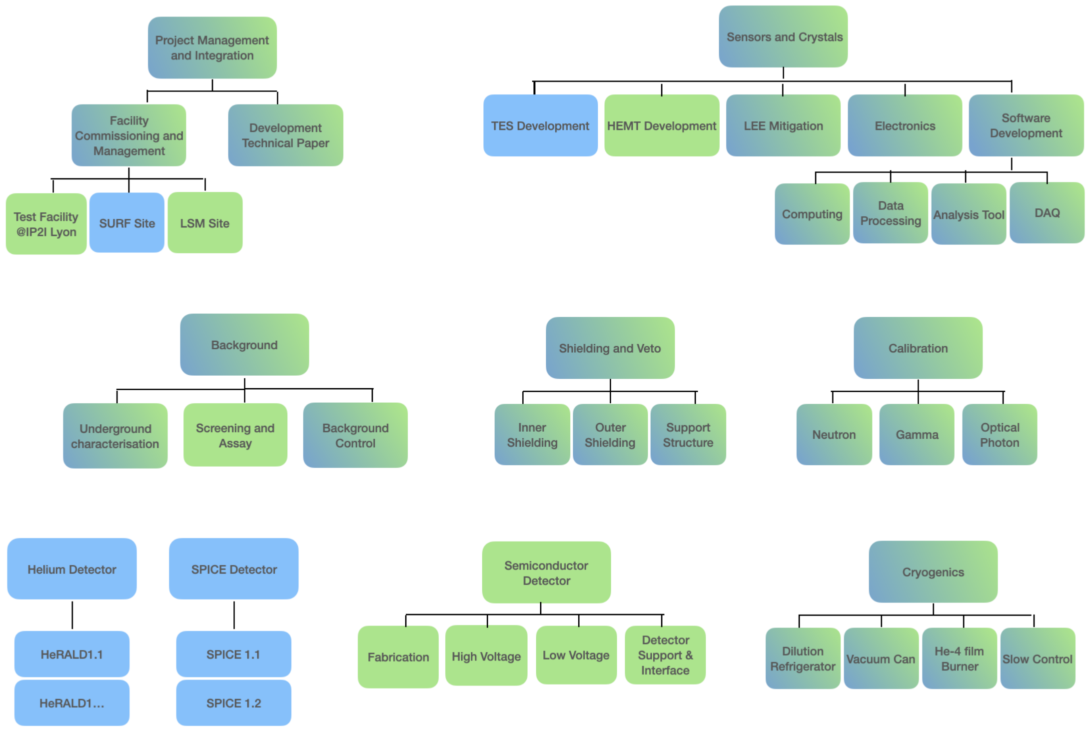


Figure 12: WBS structure for each Level1 WBS item.

**Semiconductor Detector: High Voltage** IJCLab will continue to coordinate the R&D on HV detector technology as in the context of the Cryosel-ANR program.
**Semiconductor Detector: Low Voltage** IP2I will continue to coordinate the development of this program as in the context of RICOCHET .
**Background: Underground Characterization**
The LPSC intends to coordinate this task, in continuation of its leadership role in this activity for the RICOCHET experiment. In addition to the background budget assessment, it will develop cleanliness and dust exposure protocol.
**Background: Screening and Assay**
The LPSC, with its strong connexion to the LSM screening infrastructure at LSM, intends to coordinate this activity that involves its BEGe and XIA detectors. IP2I will contribute via its involvment with the Gentiane HPGe.

# 7 Timeline, human resources and budget

**Timeline**
The following experimental schedule tentatively assumes full funding of the French activities starting in 2024. Actual resources, funding and lead times of parts will affect the actual schedule.

- 2024

  Screening activities and material selection

Finalize background budget model via Geant4 MonteCarlo
Detector R&D phases: detector design/fabrication, tests at surface cryostats
Ordering of the commercially produced parts of the refrigerator and finalization of the design of the payload stages and volumes of the cryostat

- 2025

Procurement of shield
Assembly of the infrastructure underground at LSM
Detector R&D phases: detector design/fabrication, tests at surface cryostats

- 2026

Commissioning phases of the first payload for TE-phase1
Detector R&D phases: detector design/fabrication, tests at surface cryostats
Start of science data taking at LSM

**Human resources**

The success of EDELWEISS has shown that the IN2P3 cryogenic detector groups have had, in the past, the strength and expertise to manage a leading role in the installation and exploitation of a major low-background cryogenic facility at LSM. Nowadays, with the addition of the Ricochet and CUPID experiments to the IN2P3 cryogenic detector scientific landscape, the IN2P3 TESSERACT partners (IP2I, IJCLab, and LPSC) have attracted highly qualified researchers, engineers, postdoc and students. For instance, in the last two years, with the support of IN2P3 and our laboratories, there has been 2 CNRS researcher entries at LSPC and 1 IR at IP2I. To ensure the maximal impact of the French groups in TESSERACT, together with the continuing efforts on both Ricochet and CUPID, this effort should be completed with 1) a CR entry at IP2I to consolidate the role of France in the detector development program and science output of TESSERACT, and 2) an IR recruitment at IJCLab to ensure the growing demand on fabrication and development of innovative detectors, taking into account that this laboratory will also be heavily involved in fabricating CUPID's light detectors. Additionally, care should be taken to strengthen appropriately technical support for the new experimental infrastructures at LSM. Although the TESSERACT at LSM project is just starting, and that no formal commitments have been formalized yet with the lab directorates, we are confident that the IN2P3 partners, in close collaboration with the US TESSERACT partners, have the expertise and can attract the required highly-qualified human resources to build a new world-leading low-background cryogenic dark matter experiment at the LSM.

**Budget**

As mentionned in Sec. 1.2, TESSERACT is already an existing and funded pre-project from the DOE dark matter new initiatives program. It started in 2020 and has already received so far 1.3 M€ in funds for equipment, materials, engineering, and project management. The total pre-project budget from the DOE, *i.e.* excluding resources needed to build TESSERACT at LSM, is expected to reach 2.8 M€ by 2025.

Based on the long-standing experience of both the French and US TESSERACT partners in building low-background cryogenic experiments, and quotes for the most expensive equipments, the budget for the installation of TESSERACT at LSM, starting with only one cryostat to begin with and its environment, is estimated to 1.5 M€. This includes 700 k€ for the cryostat itself, 400 k€ for the shielding (including in-kind French contribution for lead, PE and in-kind US contributions for Ti), 400 k€ for the clean room and all of the remaining equipments needed at LSM (including clean storage, wirebonders and workspaces).

The budget for the detector R&D in the initial period of the project (2024-2026) is estimated to be of 2 M€. These include:

- Significant infrastructure upgrades and new equipment for the IN2P3 laboratories essential to the project: equipment for radiopurity assay at LPSC, upgrade of IJCLab fabrication and cryogenic test facility and upgrade of the cryogenic test facility at IP2I – 1 M€ ;
- Detector materials and consumables related to the construction of the semiconducting detector arrays: Ge Crystals, HEMT developments, SQUID electronics, various electronic components, materials and fabrication costs – 1 M€.

To summarize, to get the TESSERACT at LSM project started, including the addition of the French IN2P3 detector technology to the TESSERACT payload and science reach, we need a total budget of 3.5 M€ and the support from the IN2P3 lab directorates to assign technical manpower to the project.

As of today, the French TESSERACT partners do not have any fundings. Various avenues are being explored such as internal funding scheme from the CNRS, or from the European Research Council (one Advanced ERC grant proposal has been submitted in 2023 with S. Marnieros as the PI). It is worth noticing that since July 2023 TESSERACT has become an IN2P3 master project, hence allowing for IN2P3 collaborators to work officially on this new project and ask for both manpower and financial resources to support this activity.

# 8 SWOT analysis

We present here the SWOT analysis of the TESSERACT at LSM project.

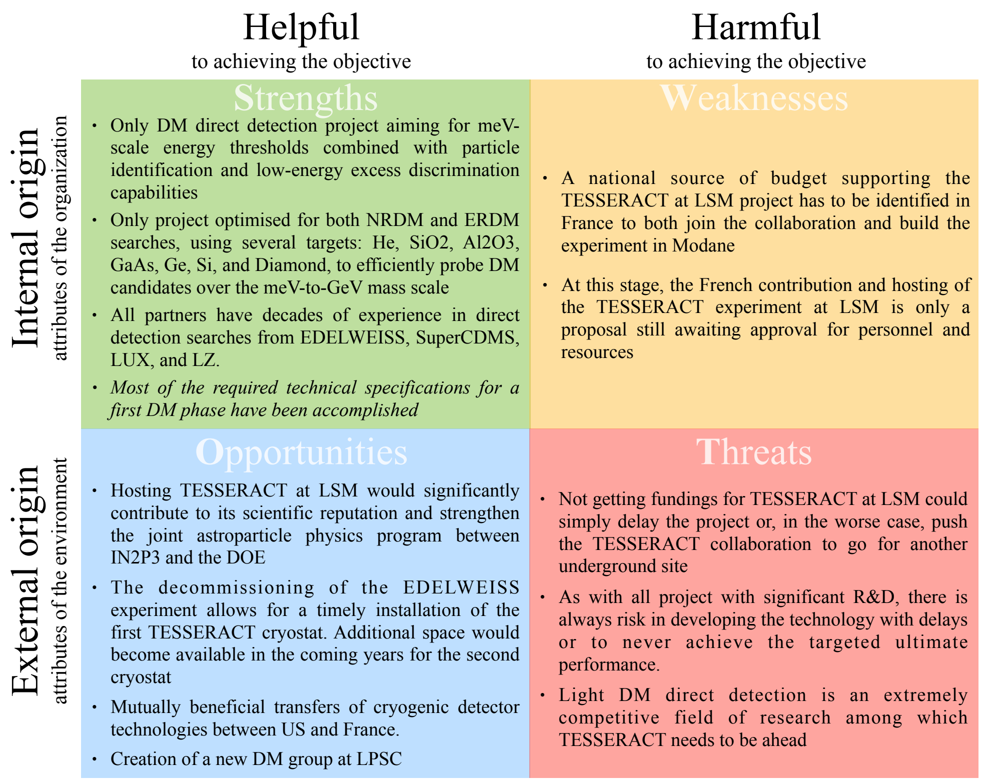


Figure 13: SWOT analysis of the TESSERACT at LSM project

# References

[1] D.S. Akerib *et al.* Results from a search for dark matter in the complete lux exposure. *Phys. Rev. Lett.*, 118:021303, Jan 2017.

[2] E. Aprile *et al.* Dark matter search results from a one ton-year exposure of xenon1t. *Phys. Rev. Lett.*, 121:111302, Sep 2018.

[3] Boveia, Antonio and Doglioni, Caterina. Dark matter searches at colliders. 68:429–459, 2018.

[4] M. Aaboud *et al.* Search for new phenomena in final states with an energetic jet and large missing transverse momentum in $pp$ collisions at $\sqrt{s} = 13$ TeV using the atlas detector. *Phys. Rev. D*, 94:032005, Aug 2016.

[5] V. Khachatryan et al. Search for disappearing tracks in proton-proton collisions at $\sqrt{s} = 8$ TeV. *JHEP*, 01:096, 2015.

[6] CMS Collaboration. For a compendium of cms searches for supersymmetry see. *https://cms-results.web.cern.ch/cms-results/public-results/publications/SUS/index.html.*

[7] ATLAS Collaboration. For a compendium of cms searches for supersymmetry see. *https://twiki.cern.ch/twiki/bin/view/AtlasPublic/SupersymmetryPublicResults*.

[8] Mohammadtaher Safarzadeh and David N. Spergel. Ultra-light Dark Matter is Incompatible with the Milky Way's Dwarf Satellites. 6 2019.

[9] Matthew J. Strassler and Kathryn M. Zurek. Echoes of a hidden valley at hadron colliders. *Physics Letters B*, 651(5):374–379, 2007.

[10] Graham D. Kribs, Tuhin S. Roy, John Terning, and Kathryn M. Zurek. Quirky composite dark matter. *Physical Review D*, 81(9), may 2010.

[11] David E Kaplan, Gordan Z Krnjaic, Keith R Rehermann, and Christopher M Wells. Atomic dark matter. *Journal of Cosmology and Astroparticle Physics*, 2010(05):021–021, may 2010.

[12] Junhai Kang and Markus A. Luty. Macroscopic strings and "quirks" at colliders. *Journal of High Energy Physics*, 2009(11):065, nov 2009.

[13] David E. Kaplan, Markus A. Luty, and Kathryn M. Zurek. Asymmetric dark matter. *Phys. Rev. D*, 79:115016, Jun 2009.

[14] Dan Hooper and Kathryn M. Zurek. Natural supersymmetric model with MeV dark matter. *Physical Review D*, 77(8), apr 2008.

[15] Nima Arkani-Hamed and Neal Weiner. LHC signals for a SuperUnified theory of dark matter. *Journal of High Energy Physics*, 2008(12):104–104, dec 2008.

[16] Jason Kumar, Jonathan L. Feng, George Alverson, Pran Nath, and Brent Nelson. WIMPless dark matter. In *AIP Conference Proceedings*. AIP, 2010.

[17] Matthew Baumgart, Clifford Cheung, Joshua T. Ruderman, Lian-Tao Wang, and Itay Yavin. Non-abelian dark sectors and their collider signatures. *Journal of High Energy Physics*, 2009(04):014, apr 2009.

[18] Yonit Hochberg, Eric Kuflik, Tomer Volansky, and Jay G. Wacker. Mechanism for thermal relic dark matter of strongly interacting massive particles. *Phys. Rev. Lett.*, 113:171301, Oct 2014.

[19] David N. Spergel and Paul J. Steinhardt. Observational evidence for self-interacting cold dark matter. *Phys. Rev. Lett.*, 84:3760–3763, Apr 2000.

[20] Jonathan L Feng, Manoj Kaplinghat, Huitzu Tu, and Hai-Bo Yu. Hidden charged dark matter. *Journal of Cosmology and Astroparticle Physics*, 2009(07):004–004, jul 2009.

[21] Sean Tulin, Hai-Bo Yu, and Kathryn M. Zurek. Beyond collisionless dark matter: Particle physics dynamics for dark matter halo structure. *Physical Review D*, 87(11), jun 2013.

[22] Hooman Davoudiasl, David E. Morrissey, Kris Sigurdson, and Sean Tulin. Unified origin for baryonic visible matter and antibaryonic dark matter. *Physical Review Letters*, 105(21), nov 2010.

[23] Jessie Shelton and Kathryn M. Zurek. Darkogenesis: A baryon asymmetry from the dark matter sector. *Phys. Rev. D*, 82:123512, Dec 2010.

[24] Matthew R. Buckley and Lisa Randall. Xogenesis. *Journal of High Energy Physics*, 2011(9), sep 2011.

[25] Z. Chacko, Hock-Seng Goh, and Roni Harnik. Natural electroweak breaking from a mirror symmetry. *Physical Review Letters*, 96(23), jun 2006.

[26] Rouven Essig et al. Snowmass2021 Cosmic Frontier: The landscape of low-threshold dark matter direct detection in the next decade. In *Snowmass 2021*, 3 2022.

[27] Romain Gaior. The DAMIC-M experiment: scientific results from prototype detector and development status. *PoS*, ICRC2023:1419, 2023.

[28] G. Angloher et al. Results on sub-GeV dark matter from a 10 eV threshold CRESST-III silicon detector. *Phys. Rev. D*, 107(12):122003, 2023.

[29] Shin-ichiro Tamura. Spontaneous decay rates of la phonons in quasi-isotropic solids. *Phys. Rev. B*, 31:2574–2577, Feb 1985.

[30] J. J. Yen, B. Shank, B. A. Young, B. Cabrera, P. L. Brink, M. Cherry, J. M. Kreikebaum, R. Moffatt, P. Redl, A. Tomada, and E. C. Tortorici. Measurement of quasiparticle transport in aluminum films using tungsten transition-edge sensors. *Applied Physics Letters*, 105(16):163504, 10 2014.

[31] Prakruth Adari *et al.* EXCESS workshop: Descriptions of rising low-energy spectra. *SciPost Physics Proceedings*, (9), aug 2022.

[32] E. Armengaud *et al.* (EDELWEISS Collaboration). Searching for low-mass dark matter particles with a massive ge bolometer operated above ground. *Physical Review D*, 99(8), apr 2019.

[33] Q. Arnaud *et al.* (EDELWEISS Collaboration). First germanium-based constraints on sub-MeV dark matter with the EDELWEISS experiment. *Physical Review Letters*, 125(14), oct 2020.

[34] Julien Billard. *Searching for Dark Matter and New Physics in the Neutrino sector with Cryogenic detectors*. Habilitation à diriger des recherches, Université Claude Bernard Lyon 1, January 2021.

[35] G. Angloher et al. Results on MeV-scale dark matter from a gram-scale cryogenic calorimeter operated above ground. *Eur. Phys. J. C*, 77(9):637, 2017.

[36] I. Alkhatib et al. Light Dark Matter Search with a High-Resolution Athermal Phonon Detector Operated Above Ground. *Phys. Rev. Lett.*, 127:061801, 2021.

[37] E. T. Mannila, P. Samuelsson, S. Simbierowicz, J. T. Peltonen, V. Vesterinen, L. Grönberg, J. Hassel, V. F. Maisi, and J. P. Pekola. A superconductor free of quasiparticles for seconds. *Nature Phys.*, 18:145–148, 2022.

[38] Sinead Griffin, Simon Knapen, Tongyan Lin, and Kathryn M. Zurek. Directional Detection of Light Dark Matter with Polar Materials. *Phys. Rev. D*, 98(11):115034, 2018.

[39] Simon Knapen, Tongyan Lin, Matt Pyle, and Kathryn M. Zurek. Detection of Light Dark Matter With Optical Phonons in Polar Materials. *Phys. Lett. B*, 785:386–390, 2018.

[40] Sinéad M. Griffin, Katherine Inzani, Tanner Trickle, Zhengkang Zhang, and Kathryn M. Zurek. Multichannel direct detection of light dark matter: Target comparison. *Phys. Rev. D*, 101:055004, Mar 2020.

[41] S. Derenzo, E. Bourret, S. Hanrahan, and G. Bizarri. Cryogenic Scintillation Properties of $n$-Type GaAs for the Direct Detection of MeV/c$^2$ Dark Matter. *J. Appl. Phys.*, 123(11):114501, 2018.

[42] A. H. Abdelhameed et al. First results from the CRESST-III low-mass dark matter program. *Phys. Rev. D*, 100(10):102002, 2019.

[43] P. M. Echenique and J. B. Pendry. Reflectivity of liquid $^4$He surfaces to $^4$He atoms. *Phys. Rev. Lett.*, 37:561–563, Aug 1976.

[44] D. O. Edwards and P. P. Fatouros. Theory of atomic scattering at the free surface of liquid $^4$He. *Phys. Rev. B*, 17:2147–2159, Mar 1978.

[45] F Dalfovo, M Guilleumas, A Lastri, L Pitaevskii, and S Stringari. Quantum evaporation from superfluid helium at normal incidence. *Journal of Physics: Condensed Matter*, 9(24):L369, jun 1997.

[46] C. Enss, S.R. Bandler, R.E. Lanou, H.J. Maris, T. More, F.S. Porter, and G.M. Seidel. Quantum evaporation of4he: Angular dependence and efficiency. *Physica B: Condensed Matter*, 194-196:515–516, 1994.

[47] R. Anthony-Petersen et al. Applying Superfluid Helium to Light Dark Matter Searches: Demonstration of the HeRALD Detector Concept. 7 2023.

[48] P. N. Luke. Voltage-assisted calorimetric ionization detector. *J. Appl. Phys.*, 64(6858):6858, 1988.

[49] B.S. Neganov and V.N. Trofimov. Colorimetric method measuring ionizing radiation. *Otkryt. Izobret.*, 146:215, 1985.

[50] D. Barker, W. Z. Wei, D. M. Mei, and C. Zhang. Ionization Efficiency Study for Low Energy Nuclear Recoils in Germanium. *Astropart. Phys.*, 48:8, 2013.

[51] E. Armengaud *et al.* (EDELWEISS Collaboration). Performance of the EDELWEISS-III experiment for direct dark matter searches. *Journal of Instrumentation*, 12(08):P08010–P08010, aug 2017.

[52] L. Hehn *et al.* (EDELWEISS Collaboration). Improved EDELWEISS-III sensitivity for low-mass WIMPs using a profile likelihood approach. *The European Physical Journal C*, 76:468, oct 2016.

[53] E. Armengaud *et al.* Measurement of the cosmogenic activation of germanium detectors in EDELWEISS-III. *Astropart. Phys.*, 91:51–64, 2017.

[54] R. Agnese *et al.* First dark matter constraints from a SuperCDMS single-charge sensitive detector. *Physical Review Letters*, 121(5), aug 2018.

[55] B. Schmidt *et al.* Muon-induced background in the EDELWEISS dark matter search. *Astroparticle Physics*, 44:28–39, apr 2013.

[56] E. Armengaud et al. Performance of the EDELWEISS-III experiment for direct dark matter searches. *JINST*, 12(08):P08010, 2017.

[57] A. Armatol et al. First cryogenic tests on BINGO innovations. In *32nd Rencontres de Blois on Particle Physics and Cosmology*, 4 2022.

[58] F.T. Avignone, R.L. Brodzinski, J.I. Collar, H.S. Miley, E. Garcia, A. Morales, J. Morales, R. Nuñez-Lagos, J.H. Reeves, C. Saenz, and J.A. Villar. Theoretical and experimental investigation of cosmogenic radioisotope production in germanium. *Nuclear Physics B - Proceedings Supplements*, 28(1):280–285, 1992.

[59] G. J. Neary and John Douglas Cockcroft. The $\beta$-ray spectrum of radium e. *Proceedings of the Royal Society of London. Series A. Mathematical and Physical Sciences*, 175(960):71–87, 1940.

[60] E. Armengaud *et al.* Performance of the edelweiss-iii experiment for direct dark matter searches. *Journal of Instrumentation*, 12(08):P08010, aug 2017.

[61] Camus Ph et al. CUTE: A Low Background Facility for Testing Cryogenic Dark Matter Detectors. *J. Low Temp. Phys.*, 193:813, 2018.

[62] W. Wilson *et al.* The cryogenic underground test (cute) facility at snolab. *Frontiers in Physisc - Special Edition Underground Laboratories.*, In Preparation, 2023.

[63] G. Angloher et al. Exploring CE$\nu$NS with NUCLEUS at the Chooz nuclear power plant. *Eur. Phys. J. C*, 79(12):1018, 2019.

[64] C. Augier et al. Fast neutron background characterization of the future Ricochet experiment at the ILL research nuclear reactor. *Eur. Phys. J. C*, 83(1):20, 2023.

[65] T. Salagnac et al. Optimization and Performance of the CryoCube Detector for the Future Ricochet Low-Energy Neutrino Experiment. *J. Low Temp. Phys.*, 211(5-6):398–406, 2023.

[66] Quan Dong, Ying-Xin Liang, D. Ferry, Antonella Cavanna, U. Gennser, L. Couraud, and Yong Jin. Ultra-low noise high electron mobility transistors for high-impedance and low-frequency deep cryogenic readout electronics. *Appl. Phys. Lett.*, 105:013504–013504, 2014.

[67] C. Augier et al. First demonstration of 30 eVee ionization energy resolution with Ricochet germanium cryogenic bolometers. 5 2023.

[68] G. Baulieu et al. HEMT-Based 1 K Front-End Electronics for the Heat and Ionization Ge CryoCube of the Future Ricochet CE$\nu$NS Experiment. *J. Low Temp. Phys.*, 209(3-4):570–580, 2022.

[69] J. Billard, L. Strigari, and E. Figueroa-Feliciano. Implication of neutrino backgrounds on the reach of next generation dark matter direct detection experiments. *Phys. Rev. D*, 89(2):023524, 2014.

[70] F. Ruppin, J. Billard, E. Figueroa-Feliciano, and L. Strigari. Complementarity of dark matter detectors in light of the neutrino background. *Phys. Rev. D*, 90(8):083510, 2014.

[71] A. Juillard et al. Low-noise HEMTs for Coherent Elastic Neutrino Scattering and Low-Mass Dark Matter Cryogenic Semiconductor Detectors. *J. Low Temp. Phys.*, 199(3-4):798–806, 2019.

[72] Q. Arnaud et al. Optimizing EDELWEISS detectors for low-mass WIMP searches. *Phys. Rev. D*, 97(2):022003, 2018.

[73] G. Angloher et al. Latest observations on the low energy excess in CRESST-III. *SciPost Phys. Proc.*, 12:013, 2023.

[74] Robin Anthony-Petersen et al. A Stress Induced Source of Phonon Bursts and Quasiparticle Poisoning. 8 2022.

[75] E. Armengaud *et al.* Search for sub-GeV dark matter via the migdal effect with an EDELWEISS germanium detector with NbSi transition-edge sensors. *Physical Review D*, 106(6), sep 2022.

[76] C. Augier *et al.* Tagging and localization of ionizing events using NbSi transition edge phonon sensors for dark matter searches. *Physical Review D*, 108(2), jul 2023.

[77] B. G. Lowe. Measurements of fano factors in silicon and germanium in the low-energy x-ray region. *Nuclear Instruments and Methods in Physics Research Section A*, 399:354–364, 1997.

[78] K. Ramanathan and N. Kurinsky. Ionization yield in silicon for eV-scale electron-recoil processes. *Physical Review D*, 102(6), sep 2020.

[79] M. Scharff J. Lindhard and H.E. Schiott. Range concepts and heavy ion ranges (notes on atomic collisions ii). *Matematisk-fysiske meddelelser: udgivet af Det Kongelige danske videnskabernes selskab*, 33:14, 1963.

[80] A. Benoit *et al.* (EDELWEISS Collaboration). Measurement of the response of heat-and-ionization germanium detectors to nuclear recoils. *Nuclear Instruments and Methods in Physics Research Section A: Accelerators, Spectrometers, Detectors and Associated Equipment*, 577(3):558–568, jul 2007.

[81] R. Agnese *et al.* (SuperCDMS Collaboration). Energy loss due to defect formation from 206pb recoils in SuperCDMS germanium detectors. *Applied Physics Letters*, 113(9), aug 2018.

[82] John N. Bahcall. Exchange and overlap effects in electron capture and in related phenomena. *Phys. Rev.*, 132:362–367, Oct 1963.

[83] H. Genz, J. P. Renier, J. G. Pengra, and R. W. Fink. Multiwire-proportional-counter measurement of the $\frac{M}{L}$ orbital-electron-capture ratio in $^{71}$Ge decay. *Phys. Rev. C*, 3:172–179, Jan 1971.

[84] H. Lattaud, Q. Arnaud, J. Billard, J. Colas, L. Dumoulin, M. De Jésus, A. Juillard, J. Gascon, S. Marnieros, and C. Oriol. Phonon and charge signals from IR and x excitation in the SELENDIS ge cryogenic detector. *Journal of Low Temperature Physics*, 209(3-4):263–270, sep 2022.

[85] A. Biekert *et al.* (SPICE/HeRALD Collaboration). A portable and monoenergetic 24 keV neutron source based on $^{124}$sb-$^{9}$be photoneutrons and an iron filter. *Journal of Instrumentation*, 18(07):P07018, jul 2023.

[86] L. Thulliez *et al.* Calibration of nuclear recoils at the 100 eV scale using neutron capture. *Journal of Instrumentation*, 16(07):P07032, jul 2021.

[87] H. Abele *et al.* Observation of a nuclear recoil peak at the 100 eV scale induced by neutron capture. *Physical Review Letters*, 130(21), may 2023.